

## Master Thesis

# Design and Control of an Aerial Layouting Tool

Autumn Term 2021

---

**Supervised by:**

Christian Lanegger  
Marco Tognon

**Author:**

Marco Ruggia



## **Declaration of Originality**

I hereby declare that the written work I have submitted entitled

### **Design and Control of an Aerial Layouting Tool**

is original work which I alone have authored and which is written in my own words.<sup>1</sup>

#### **Author(s)**

Marco Ruggia

#### **Student supervisor(s)**

Christian Lanegger  
Marco Tognon

#### **Supervising lecturer**

Roland Siegwart

With the signature I declare that I have been informed regarding normal academic citation rules and that I have read and understood the information on 'Citation etiquette' (<https://www.ethz.ch/content/dam/ethz/main/education/rechtliches-abschluesseliste/leistungskontrollen/plagiarism-citationetiquette.pdf>). The citation conventions usual to the discipline in question here have been respected.

The above written work may be tested electronically for plagiarism.

31.12.2021  
Place and date

Marco Ruggia  
Signature

<sup>1</sup>Co-authored work: The signatures of all authors are required. Each signature attests to the originality of the entire piece of written work in its final form.



---

# Contents

## Abstract

<b>1</b>	<b>Introduction</b>	<b>1</b>
1.1	Framework . . . . .	2
1.2	Related Literature . . . . .	3
<b>2</b>	<b>Concept</b>	<b>4</b>
<b>3</b>	<b>Design</b>	<b>6</b>
3.1	Stewart Platform . . . . .	7
3.1.1	Optimization . . . . .	8
3.1.2	Static Validation . . . . .	9
3.1.3	Dynamic Validation . . . . .	11
3.2	Omni-Wheels . . . . .	16
3.3	Camera . . . . .	18
3.4	Drawer . . . . .	22
3.5	Auxiliary Components . . . . .	23
<b>4</b>	<b>Control</b>	<b>24</b>
4.1	Planner Node . . . . .	25
4.2	Wheels Node . . . . .	26
<b>5</b>	<b>Test-Flights</b>	<b>27</b>
5.1	Free-Flight Test . . . . .	29
5.2	Baseline Test . . . . .	30
5.3	Contact Test . . . . .	31
5.4	Compliance Test . . . . .	32

5.5	Actuator Test . . . . .	32
5.6	Feedback Test . . . . .	33
5.7	Complete Test . . . . .	33
5.8	Other Data . . . . .	34
<b>6</b>	<b>Conclusion</b>	<b>42</b>
<b>7</b>	<b>Outlook</b>	<b>43</b>
	<b>Bibliography</b>	<b>44</b>



# Abstract

Layout lines in construction sites mark the precise locations where a task should be performed. This project explores the possibility of using an aerial platform to draw these layouting lines, with surfaces for drawing being restricted to smooth ceilings. The approach taken is to use an omnidirectional micro aerial vehicle (OMAV) with a tool attached to compensate for position errors. Various tool configurations are designed and tested, revealing their influence on drawing error. The best tool configuration reaches a maximum error in the low millimeter range, meeting the project goal.



# 1 Introduction

The goal of this project is to extend the capabilities of an existing *omnidirectional micro aerial vehicle* (OMAV), to draw precise layouting lines. The standout characteristic of an OMAV is that, unlike traditional multicopters, it is able to decouple position from orientation motion and can exert forces in any direction. This makes them particularly suited for coming into contact with their environment, while maintaining stability and controllability. The OMAV in question is a variable-tilt hexacopter design, meaning it can actively tilt each of the rotor arms. Its name is *Ouzel* and it was developed by the Autonomous Systems Lab (ASL) at ETH Zürich.



Figure 1.1: Image of the *Ouzel* OMAV platform

Motivating this project is a common problem in construction sites. Layouting lines are applied to walls, ceilings and floors to mark the location of features like holes, cutouts, mounting points, chasings, etc. The Layouting lines are sometimes drawn by hand, which poses a problem when the location is out of reach. This project aims to provide a new solution by having an OMAV do the layouting autonomously.

This report will cover the entire design process, starting with the framework defining the project requirements and constraints. The concept decisions will be presented with their motivations, and the design process of the physical components described in detail. A chapter is then dedicated to the control of the layouting tool. The results are presented in the form of testflights, that not only test for the project goals, but also provide insight to the effect of each of the concept decisions.

## 1.1 Framework

The Framework for this project is defined by the performance requirements on the finished product and by the capabilities of the unmodified OMAV platform *Ouzel*. Constraints are put in place to keep the scope within reach of a one-person master thesis.

### Performance Requirements

- **Surface type**

The surfaces on which the layouting lines are made must be limited to ceilings, excluding walls, floors and corner regions. The ceiling is required to be a smooth surface without holes or other major imperfections.

- **Line characteristics**

Lines with a width no more than 3mm must be drawn within no more than 5mm of the intended position. The lines can be curved, contain corners and/or be interrupted. No restrictions are placed on the draw speed, nor the maximum draw distance.

### Platform Capabilities

- **State estimation**

A system for measurement of position and attitude of *Ouzel* is provided, with the measurements regarded as known good. For in-house tests a *Vicon* motion capture system is used, while for field operation a mobile *Laica* system will be implemented outside the scope of this project.

- **Positioning accuracy**

In free flight *Ouzel* is able to stay within 35mm of the desired position and within 10° of the desired attitude at all times. When in contact these values are expected to be roughly halved.

- **Payload capacity**

*Ouzel* is able to carry a payload of preferably no more than 1kg to preserve its performance. Constraints on the location of the center of mass are present, but unknown. As such the height of any payload should be kept low.

The main challenge of this project is to precisely move a drawing implement along a path on the ceiling. Previous efforts have indicated that *Ouzel* alone, with a marker rigidly fixed to its body, can not reach the required line precision [1]. The avenue chosen for this project is to attach a tool to *Ouzel* that compensates for any inaccuracy.

No changes are made to *Ouzels* design or its controller. Instead, the setpoint tracking difficulties of *Ouzel* are seen as mean of making the effect of the layouting tool more apparent. These difficulties are not necessarily a characteristic of all OMAVs and it is likely that improvements could be made.

## 1.2 Related Literature

The task of this project falls into the field of aerial robot manipulation. It is a quickly growing field, due to its many applications in inspection, maintenance and structure assembly. Multiple literature reviews have been published that have collected the research performed until recently [2, 3]. They conclude that many projects use OMAVs as their platform, as the underactuation of traditional multicopters is very limiting. OMAVs come in mainly two designs, fixed-tilt designs where the rotors are fixedly tilted in a nonparallel fashion, and variable-tilt designs where the rotor arms can be actively rotated. *Ouzel* falls into the later category. For manipulator arms many different designs are found, ranging from rigid arms, to series or parallel manipulators with up to six degrees of freedom (DoF). The endeffectors come in a huge variety of designs, based on the many possible tasks, that is to large to quickly summarize.

The task at hand for this project is more specifically part of push-and-slide interactions. Publications with that focus include previous work at ALS where *Ouzel* draws with a rigid arm [1]. An effort to improve on the rigid design is made by using a delta arm on a traditional quadcopter with impressive results [4]. Alternatively, a fixed-tilt OMAV with a 2 DoF series and a point contact is tried with some success [5]. A different approach is taken by the *AeroX* [6] project, that uses a fixed-tilt OMAV with a slightly compliant arm and a four wheeled endeffector using tank drive.

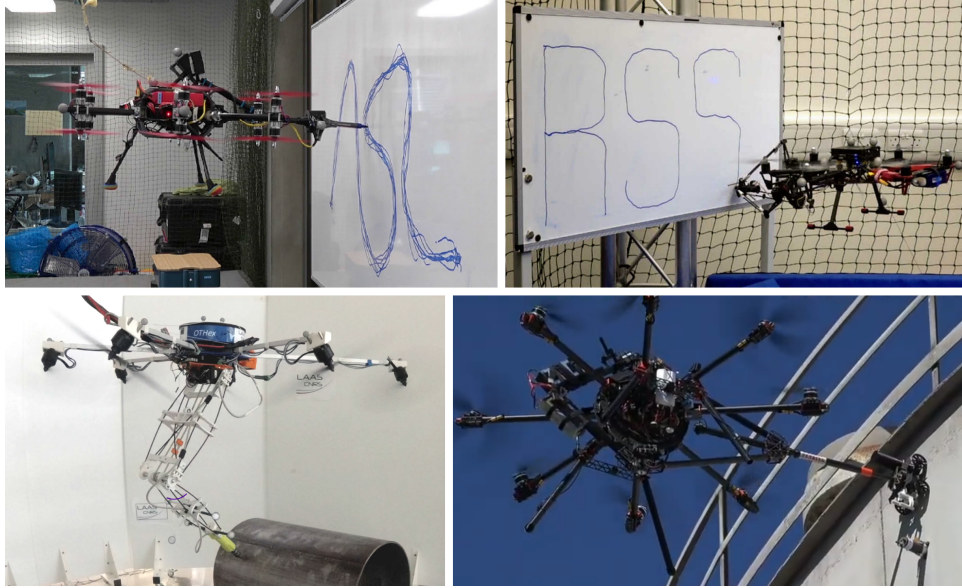


Figure 1.2: Related Designs ([1], [4], [5], [6] in reading order)

None of the found publications reach endeffector positioning accuracy as high as is required from this project. As such it is thought that this accuracy is yet unreachd.

## 2 Concept

The central part of the concept is the way in which it intends to correct disturbances in the position of the drawing implement. Below are listed the main concept decisions, each one of which adds more complexity in exchange for presumably higher likelihood of meeting the design requirements. The necessity of each one is later explored in the chapters on validation. While other concepts have been considered, only the ones that are implemented are listed here. These are thought to be the ones most likely to succeed.

### Contact

The first decision is to use at least three contact points with the ceiling. In that way roll, pitch and z-axis movement can be stabilized by simply keeping contact. Since it is expected that the disturbances are somewhat coupled, this is likely to also positively affect the yaw, x- and y-axis disturbances.

### Compliance

To improve the reliability of the contact, some compliance is added between the contact points and the drone body. This compliance has the aim to not transmit large drone disturbances to the contact points and to soften the ones it does.

The compliant structure is realized with six spring-dampers arranged as a Stewart platform. This choice allows movement in all six degrees of freedom (DoF), while maintaining some passive stability, being easy to tune and having a compact & simple design. The rigid body that sits above the compliant structure and contains the contact points and drawing implement is henceforth called "plate".

### Actuators

For more precise positioning of the plate, actuated wheels are used at the contact points. This enables the tool to drive on the ceiling. A high friction with the ceiling has the consequence that disturbances are passively suppressed, since a wheel without slip can stay on track without changes in actuation even under disturbing forces.

A common alternative design with the same intention is to use actuators to move the plate relative to the drone with e.g. a delta arm. This is deemed an inferior solution, as it requires low friction with the ceiling, so that the actuators move the plate while the drone is largely unaffected instead of the undesired opposite. With such a setup any disturbance in the drone would need to be actively suppressed by the actuators. This is thought to be much more difficult to implement reliably.

For implementation, an arrangement of three omni-directional wheels is chosen. It is the simplest solution found to also allow arbitrarily tight corners to be driven.

## Feedback

With the plate being decoupled from the drone and moving independently, it becomes necessary to track its position and correct for errors. Not doing so could lead to slow drifting of the plate relative to the drone.

For this project it is unfeasible to use the same type of state estimation as for the drone on the plate, because of the close proximity of the plate to the ceiling and occlusion by the drone. While the tracking is barely possible with the fixed *Vicon* system and smart camera placement, it is very unlikely to work with the upcoming mobile *Laica* system. The alternative chosen is to measure the relative position of the drone to the plate and to derive the plate position from it. Given the high accuracy needed to reach the required line precision, a vision based pose estimation is chosen. For that, a camera is mounted on the drone pointing at the plate and the plate is painted with a recognizable pattern.

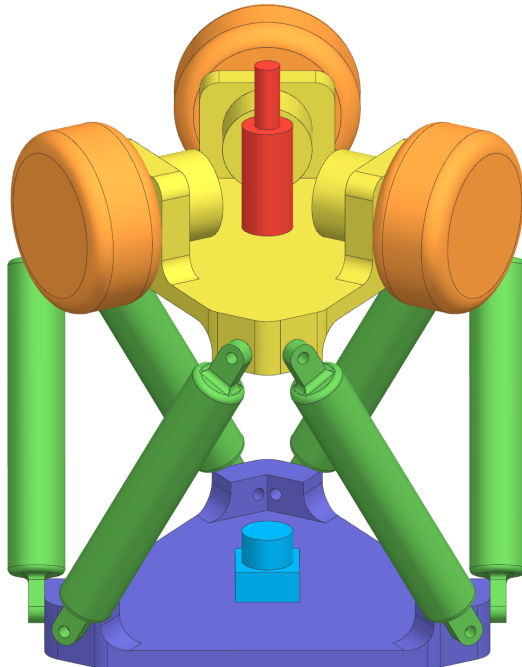


Figure 2.1: Concept mockup: Drawer (red), omni-wheels (orange), plate (yellow), Stewart platform (green), camera (blue), drone base (violet).

# 3 Design



Figure 3.1: Image of the finished tool mounted on top of *Ouzel*

The design process for all the components is described in this chapter. These components are, the Stewart platform for compliance, the omni-wheels for actuation, the camera for feedback and the drawer for drawing. In addition a short section is appended for auxiliary components. Each section will cover the requirements of the component, design methods used and a description of the resulting assembly.

### 3.1 Stewart Platform

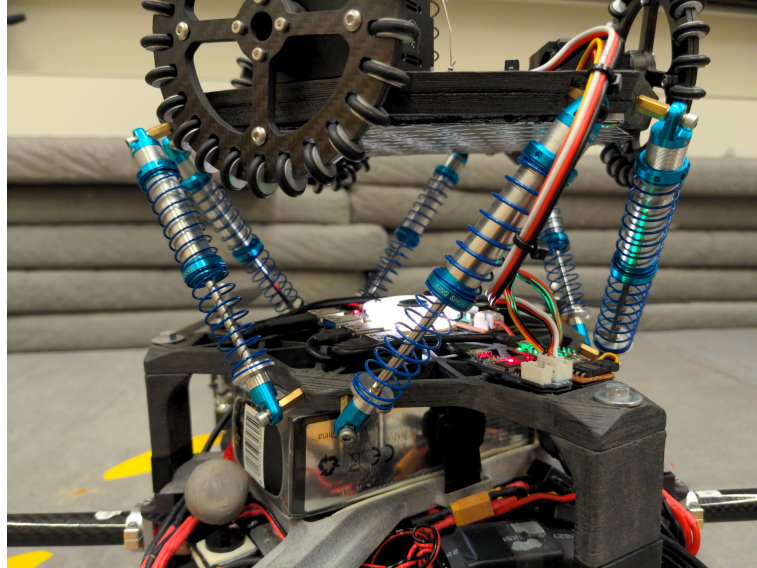


Figure 3.2: Image of the finished Stewart Platform

With the goal of the Stewart platform being to introduce compliance, its primary requirement is to allow relative plate-to-drone movement encompassing the positioning accuracy of the drone. A secondary goal is to passively stabilize the drone, meaning that, assuming the plate to be fixed in space and the drone to be pushing straight up with a constant force, the drone should find an equilibrium directly below the plate in level flight. The third goal is to dampen movement of the drone.

The spring-dampers used are *RC4WD King Off-Road Dual Spring Shocks* for radio controlled model cars. The length is chosen to place the movement range of the platform in the correct ballpark. Spring stiffness is picked such that the platform produces approximately 15N of force when mid-compression. This value is chosen as a trade-off between available thrust and ceiling grip. The damping fluid is water as it's found to be the only fluid to approach the rebound speeds needed to maintain ceiling contact with the given spring stiffness.

extended length	120 mm	spring constant	0.2 N/m
compressed length	80 mm	damping constant	0.2 N/(m/s)

Table 3.1: Spring-damper characteristics

Since the placement of the spring-dampers is thought to have a large influence on the Stewart platforms stability, an extensive analysis is undertaken. The analysis starts by finding the optimal spring-damper placements given a certain scoring metric. The resulting geometry is then further analyzed for static stability to show the validity of the chosen metric. To give more confidence that the platform stability is robust enough to work on the real system, a third analysis is performed by simulating the dynamic behaviour with a simplified drone model.

### 3.1.1 Optimization

The platform geometry is parametrized in such a way as to cover all configurations with three-fold rotational symmetry. For each configuration the drone is modelled as exerting a constant force along the z-axis, such that the equilibrium lies where the spring-dampers are at the center of their travel range. The plate is always assumed stationary. To assign a stability score to each configuration, the energy field of the drones movement in its six DoF is analyzed. This energy is calculated as the sum of the energy stored in the spring contraction and the potential energy of the z-axis force. The metric chosen for the stability score is the smallest eigenvalue of the Hessian of this energy field at the equilibrium point. This score describes the worst-case local change in energy along any movement direction.

There are two notable details to mention. This analysis implicitly equates change in position to change in attitude in its score, as the six dimensional energy space is composed of three position and three attitude dimensions. In practice the two types of measurements are scaled such that a 1mm change in position is equivalent to a 1° change in attitude. Different scalings can put different priorities over position stability vs. attitude stability. The second note is about the applicability of this analysis to ordinary multicopters. Unlike OMAVs, their thrust force always follows their orientation, which means that the thrust does not produce the conservative force field assumed for this analysis.

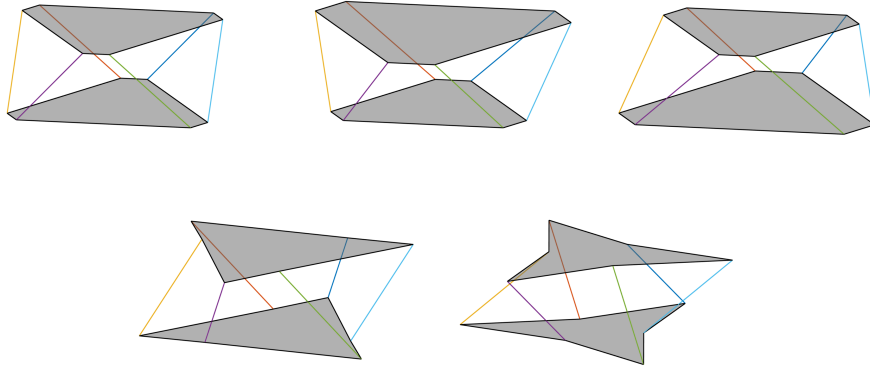


Figure 3.3: Selection of a few Stewart platform configurations

Calculating the desired platform geometry becomes an optimization problem of finding the geometry with the highest stability score. This is achieved by finely sampling the entire parameter space up to a scale where manufacturing tolerances would negate further optimization. To ensure that the platform can feasibly be built some constraints are placed on the possible parameters. Two of these constraints are active at the optimum. The maximum radial extent is reached, that limits the size of the platform, and so is the minimum height, which is put in place to keep a balance between vertical and horizontal movement range. The optimal configuration is shown in the figure below.

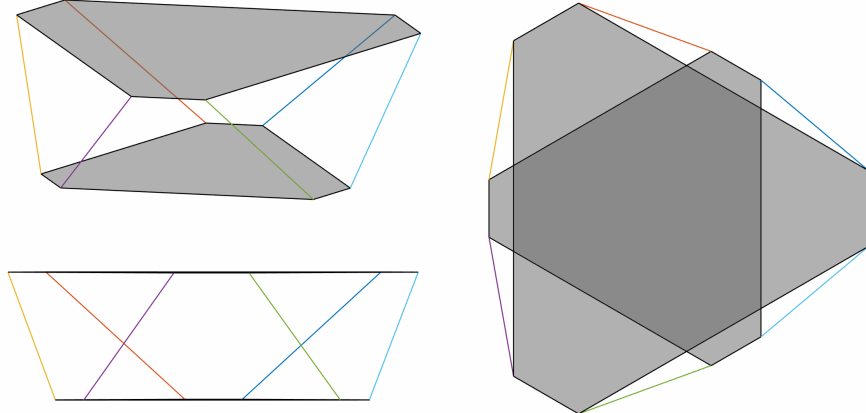


Figure 3.4: Optimal Stewart platform configuration

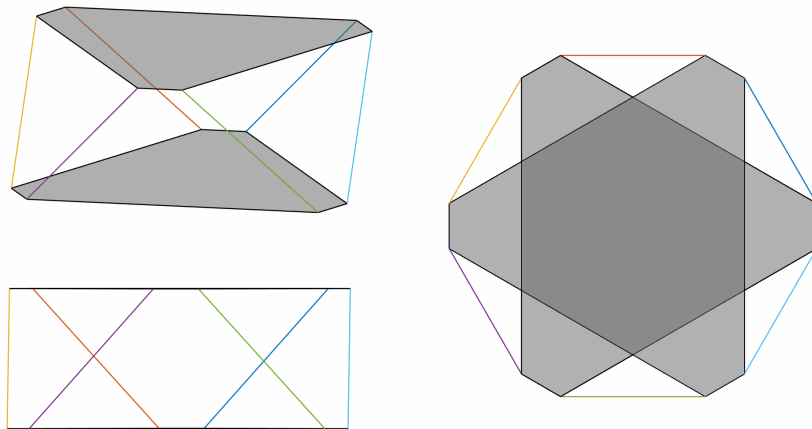


Figure 3.5: Naive Stewart platform configuration

### 3.1.2 Static Validation

Since this optimization only concerns itself with stability at the equilibrium, a second analysis is performed to ensure that the stable behaviour encompasses the entire movement range. It is done by visually inspecting plots of the energy field. Three types of plots are shown. The first plots the energy vs. position assuming that attitude stays level, the second plots energy vs. position assuming the attitude is at equilibrium for that position, and the third plots that equilibrium attitude angle vs. position. All of these are split into X-Y, X-Z & Y-Z sections.

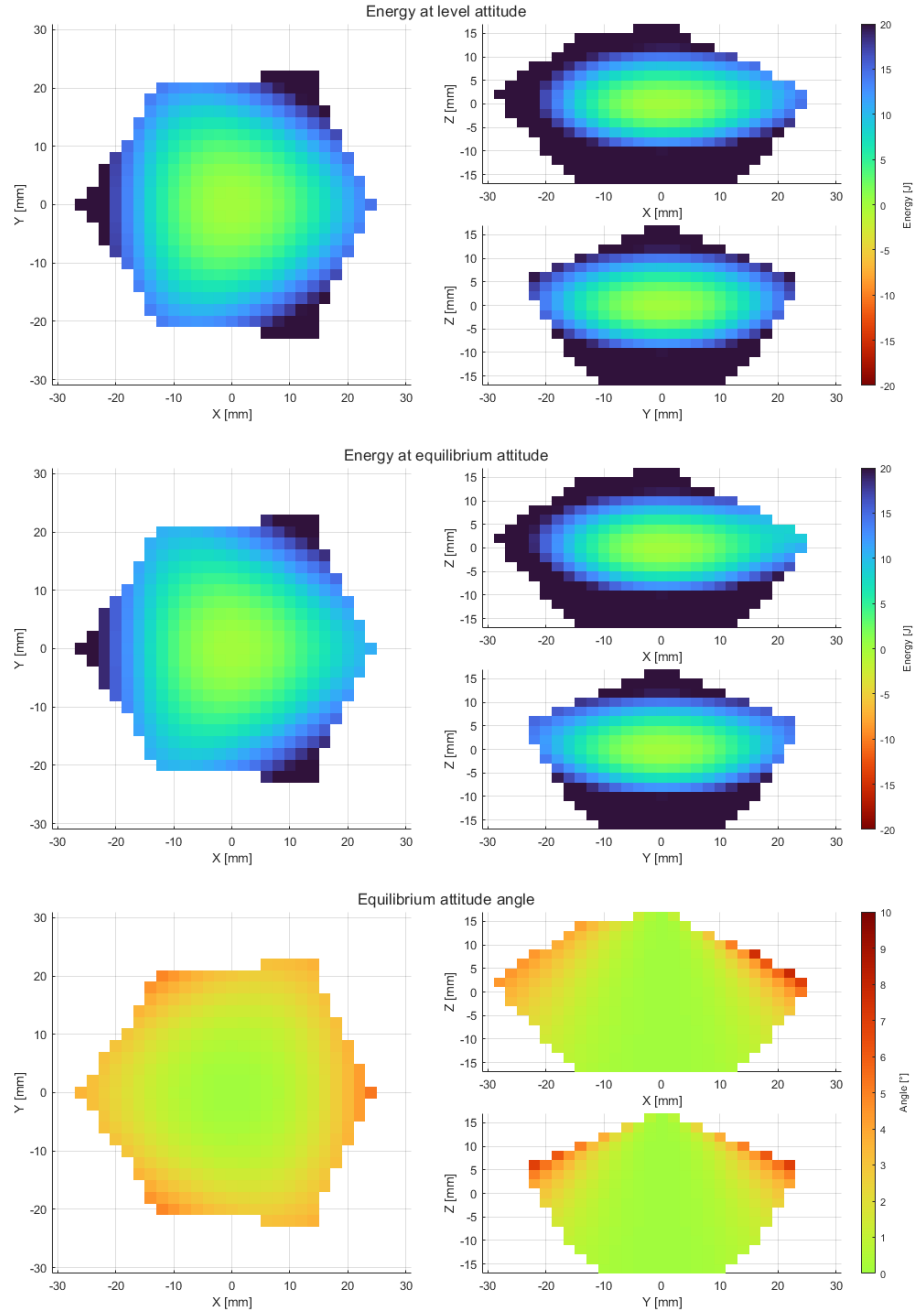


Figure 3.6: Energy plots of optimal Stewart platform configuration

As can be seen from these plots, the optimal configuration does indeed appear to exhibit stability across its entire movement range.

A naive approach may suggest to skip this analysis and to instead use a Stewart platform where the top and bottom are of equal size and spacing. The below plots show that this configuration is not stable if the attitude is left free to reach its equilibrium, but is stable in position, assuming that the attitude is kept perfectly level. As such the naive configuration is significantly inferior to the optimal configuration.

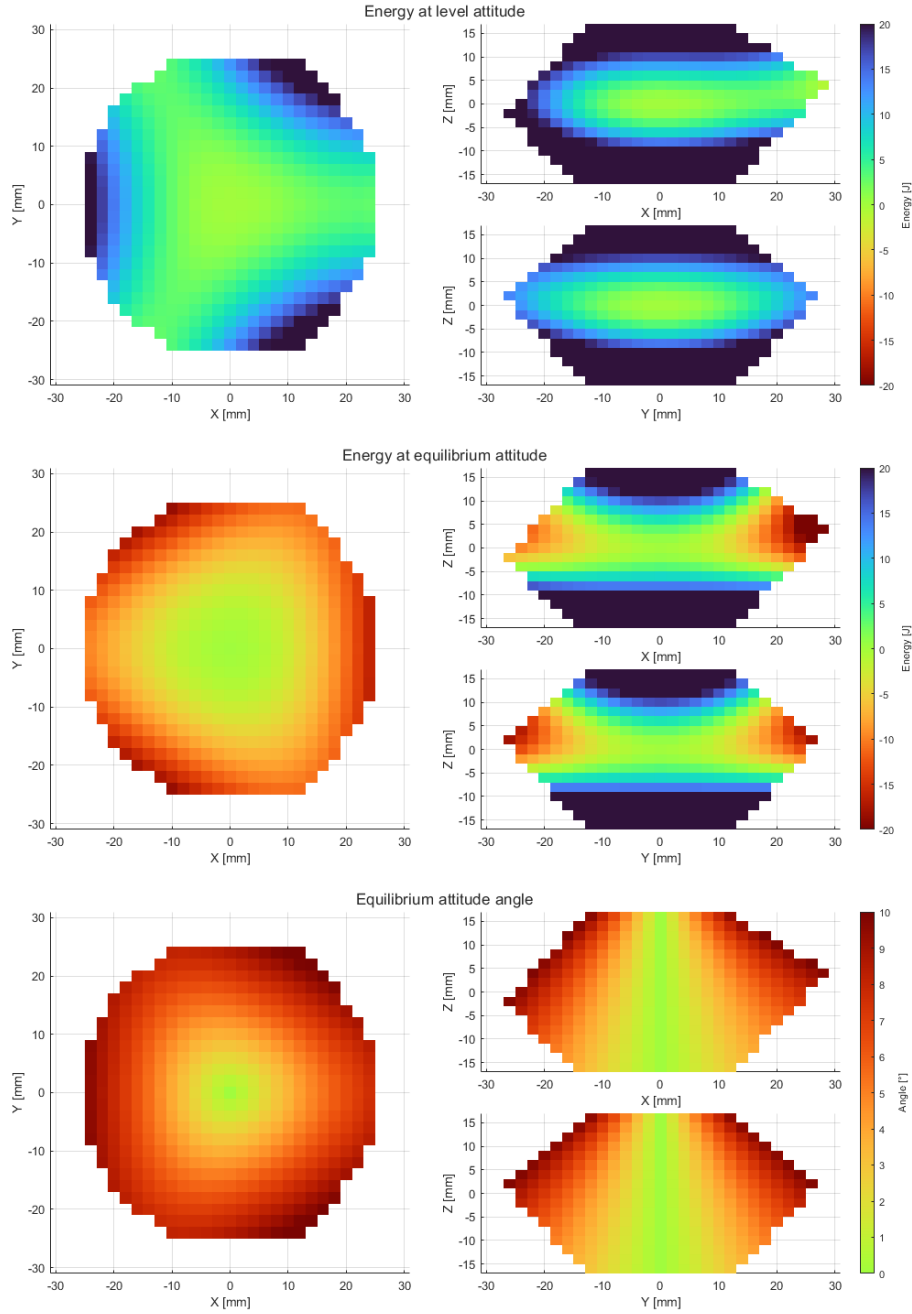


Figure 3.7: Energy plots of naive Stewart platform configuration

### 3.1.3 Dynamic Validation

While the static analysis shows that the optimal Stewart platform is stable, it does not directly allow to determine if the platform is robust to disturbances during normal operation. For that purpose a dynamics simulation environment is set up, where the interplay of platform and drone, subject to inertial forces and disturbances, can be approximated.

For the simulation, the plate and the drone are assumed to be two rigid bodies, modelled using the second law of motion and Euler's equations, resulting in 12 equations of motion (EoM) linking the 12 states with 12 external forces and torques. The input to the system comes in the form of forces and torques that can be applied to the drone. Disturbances are added to each EoM in the form of colored noise. The spring-dampers of the Stewart platform are modelled as perfect springs in parallel with perfect dampers. The travel limits are simulated by adding very strong penalty springs that push back when outside the limits.

A large simplification is made when modelling the ceiling contact, by imposing a contact constraint. In practice this is accomplished by flipping the concerned EoM's, such that it is no longer a known external force/torque that determines the evolution of a state, but a known state that determines the evolution of an external force/torque. A loss of contact can then be inferred if the contact force in z direction becomes positive or its attack point leaves the support base formed by the omni-wheel contact points. This simplification is made following the reasoning in the wheel actuators concept decision, that precise plate control on the real system is not difficult.

The continuous time system described above is discretized using the backward differentiation formula of second order (BDF2). It is chosen, because of its good accuracy and stability when solving very stiff equations, like the ones that appear at the travel limits of the spring-dampers. The discretized EoM are then solved by a nonlinear equations solver using Powell's dog leg method. The solution to the discretized EoM is the state of the plate and the drone after one timestep.

After every simulated timestep the drone controller is used to determine the next system input. The system state provided to the controller as feedback is delayed by a few timesteps and noise is added to replicate a realistic behaviour. For the controller itself, a PD design is used, which is closely related to the impedance controller used in the real drone.

The setpoint trajectory used is a tight circle path that is travelled at constant and fairly high speed while the attitude setpoint stays level. This rather simple trajectory is chosen because it causes inertial forces in all directions.

velocity on circle	$160 \text{ mm/s}$
centripetal accel.	$250 \text{ mm/s}^2$
disturbances force	$2 \text{ N}$
disturbances torque	$0.2 \text{ Nm}$

Table 3.2: Simulation parameters

Three tests are presented from this simulation environment. One with the system in its nominal configuration, one with the drone position control disabled, and one with both position and attitude control disabled. This progression puts progressively higher demands on the stabilizing properties of the Stewart platform. The first two are a success, while the disturbances in the uncontrolled configuration overpower the Stewart platform. This result passes the dynamic validation.

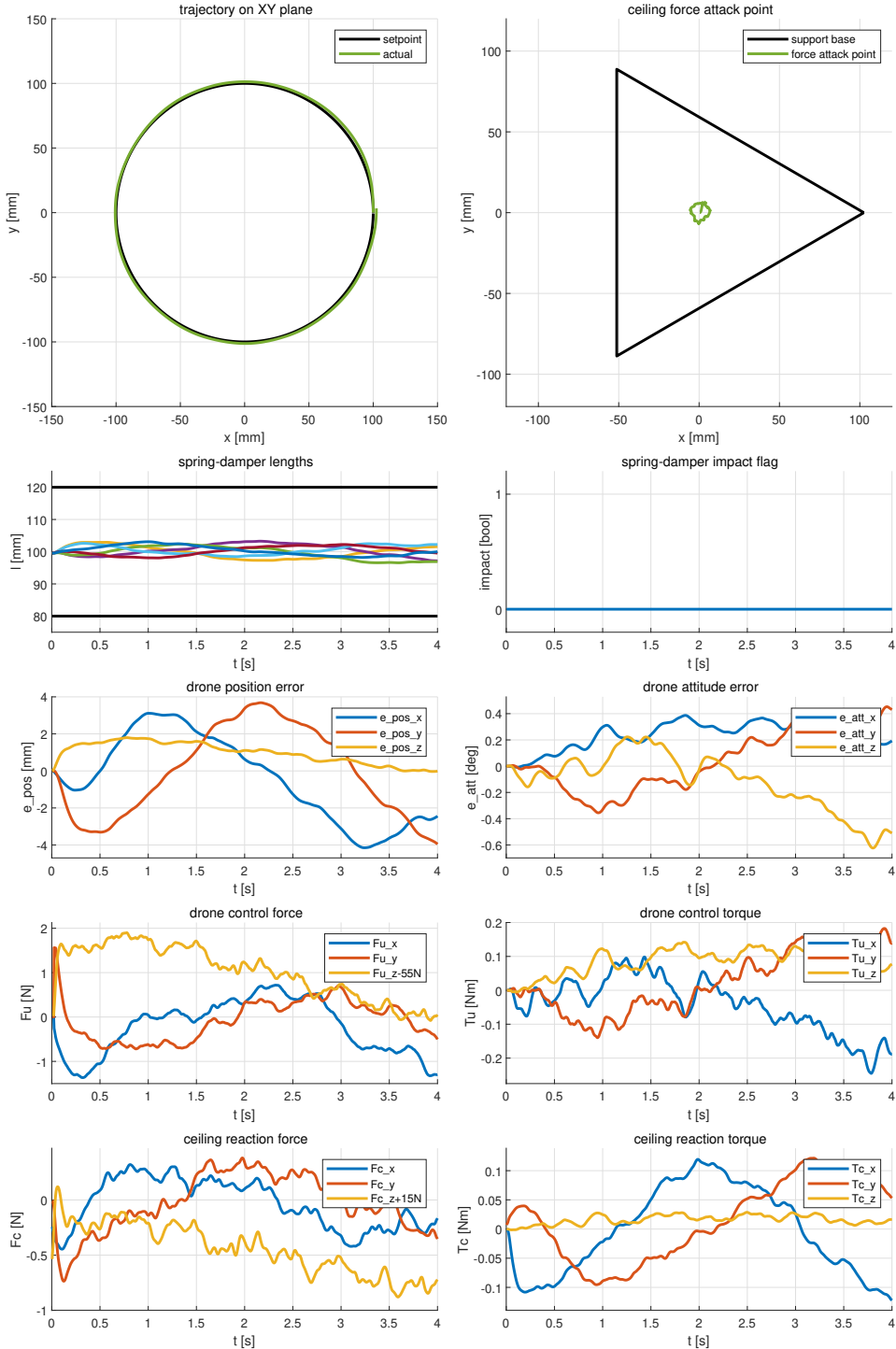


Figure 3.8: Simulation-Test 1 - Nominal control

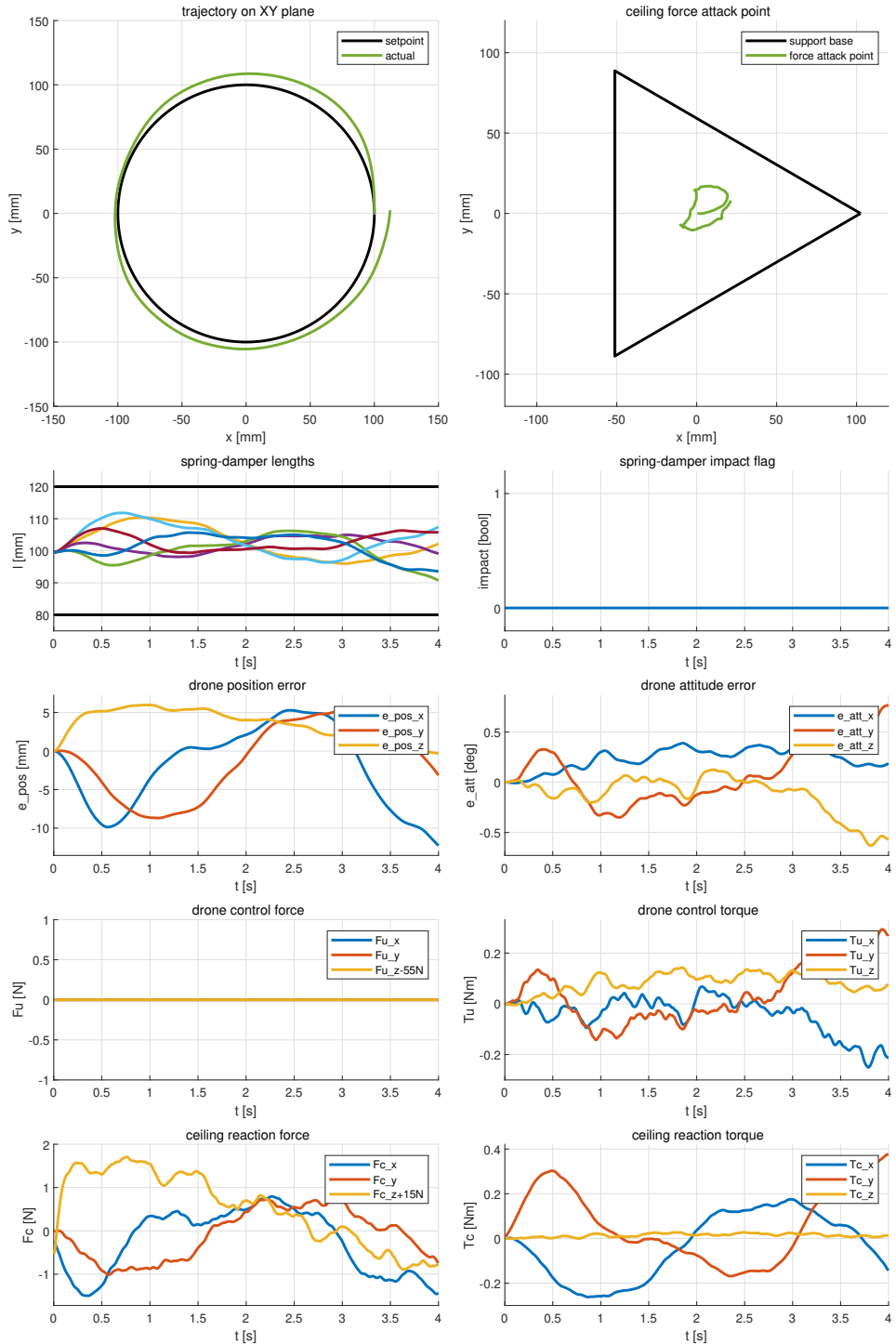


Figure 3.9: Simulation-Test 2 - Attitude only control

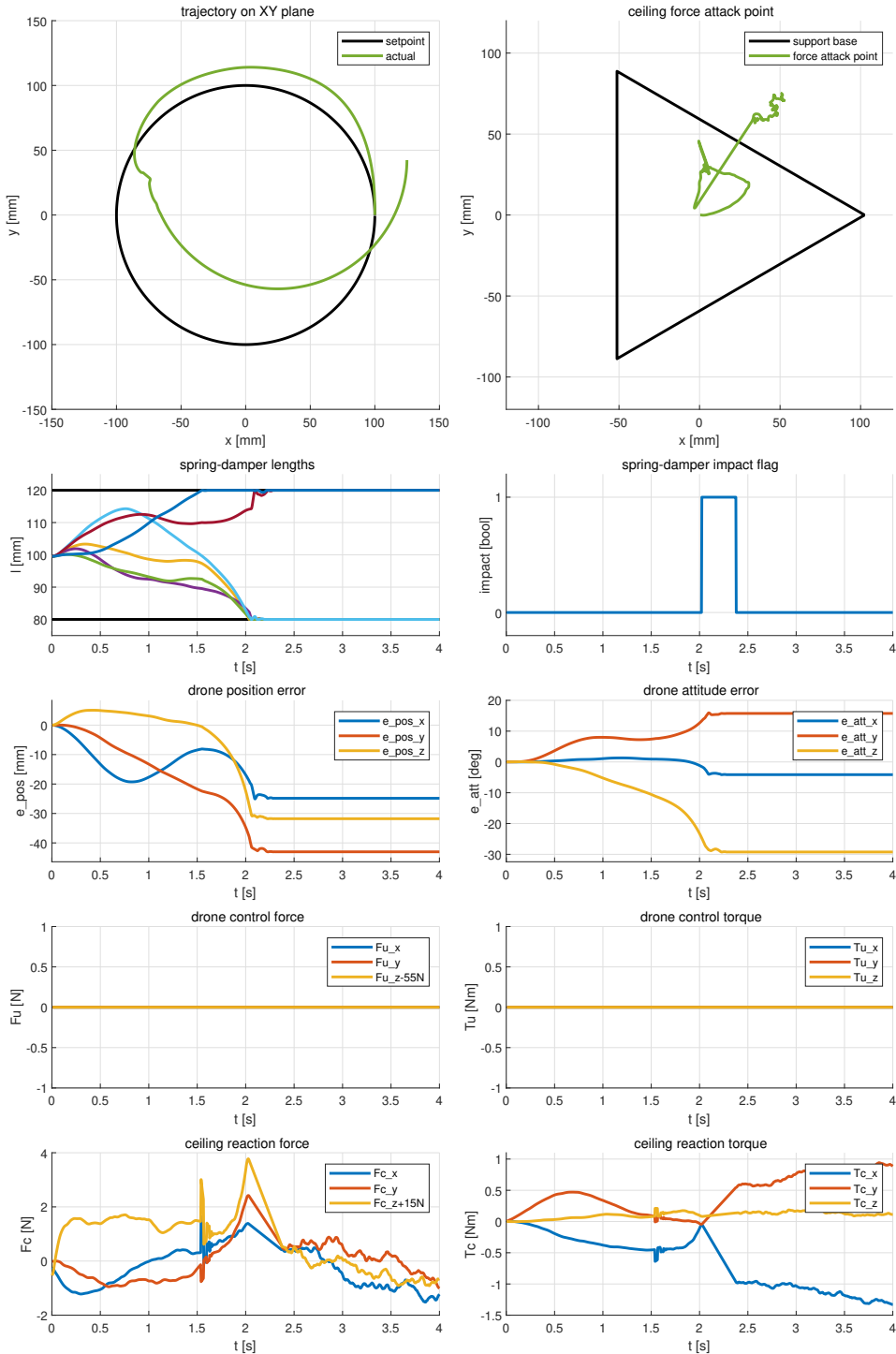


Figure 3.10: Simulation-Test 3 - No position nor attitude control

### 3.2 Omni-Wheels

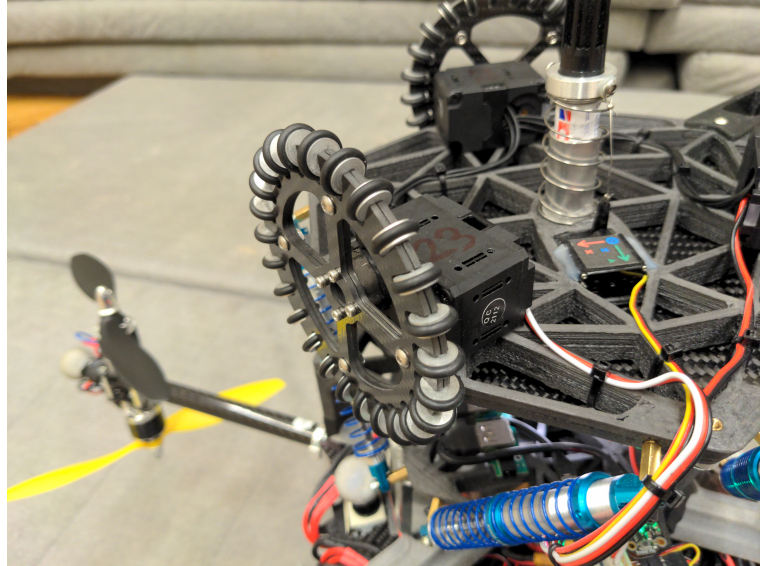


Figure 3.11: Image of a finished omni-wheel

The omni-wheels fit into the concept by enabling the tool to drive on the ceiling in any direction. To accomplish their role a couple of requirements are placed on them. Firstly, the actuators need to have sufficient torque and positioning accuracy. Secondly, the wheels need to be such as to allow smooth movement without losing grip. And Thirdly, this assembly needs to be light, as it's located far from the drone's center of mass and the Stewart platform analysis has found that increased weight negatively affects its stability. Assigning meaningful numbers to these requirements is difficult, so a trial and error approach is used instead.

The requirements of the omni-wheel actuators are similar to the requirements of the actuators driving *Ouzels* tiltable rotor arms. Due to the advantages this poses for sourcing and integration the same actuators are picked, knowing that the manufacturer *Dynamixel* also produces higher torque versions with the same mounting points if more torque was to be needed.

The model number of the *Dynamixel* actuators is *XL430-W250-T*. They are connected to *Ouzel* via USB through a *Dynamixel U2D2* communication converter, and are powered by a switching regulator to directly step down the main battery voltage.

Finding suitable omni-wheels is more difficult, as all models found online are unnecessarily heavy. For that reason custom ones are built based on a design from *GTF Robots*. The wheel diameter is 100mm to try and strike a balance between smooth running, positioning resolution and packaging constraints. The wheel hub is milled from carbon fiber reinforced polymer (CFRP) sheets, while the secondary wheels are turned from aluminium rods with soft o-rings inserted for their running surface. The weight of one such wheel is 45g, compared to the 125g of the reference *GTF* wheel. An exploded view of the assembly is shown below to explain how this design is built internally.

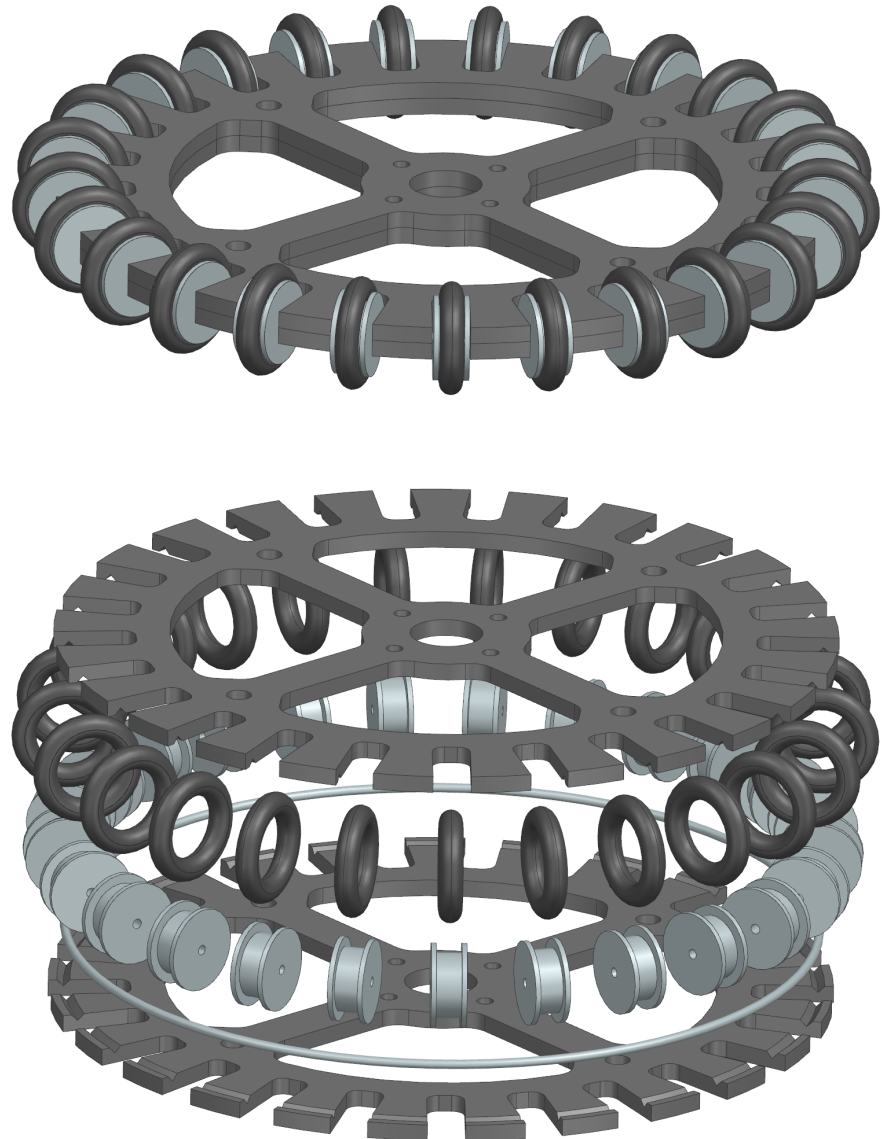


Figure 3.12: Exploded view of the omni-wheel assembly

### 3.3 Camera

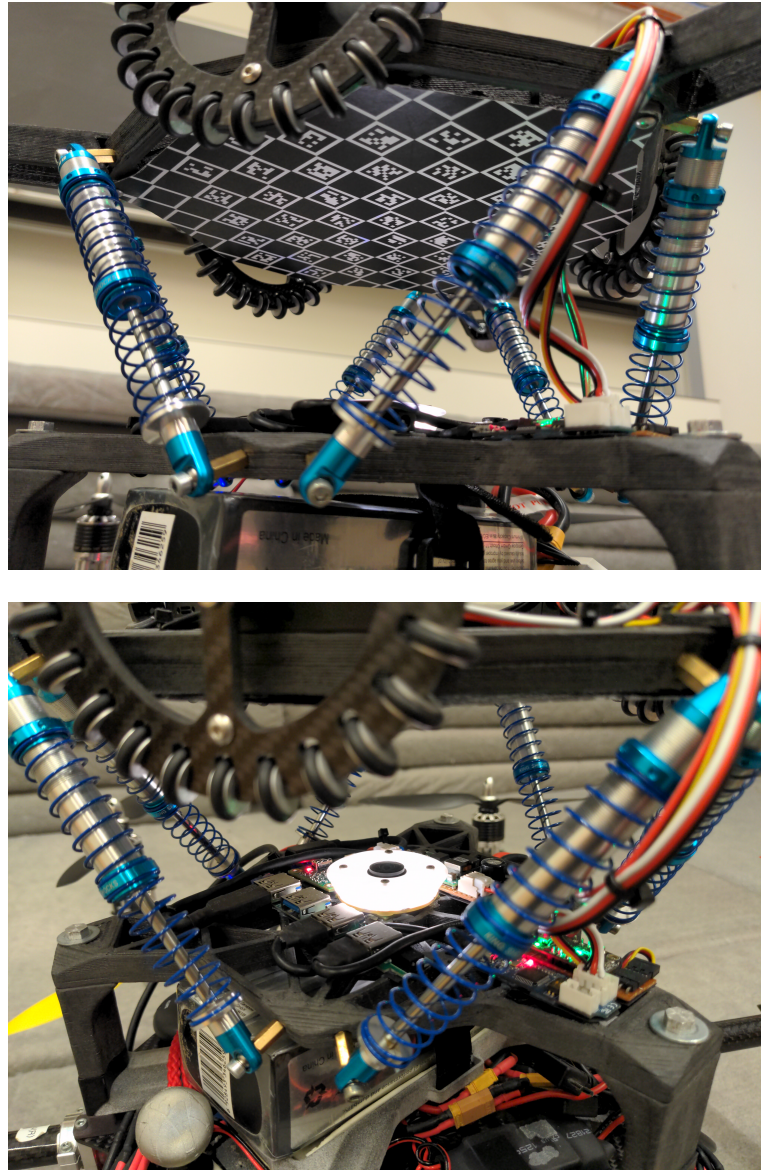


Figure 3.13: Images of the finished fiducial board and camera

To reiterate, the role of the camera is to measure the relative position between drone and plate, so that the plate pose can be derived from the known drone pose. This is needed as a feedback for the omni-wheel actuators to avoid plate drift. As such, this system needs a resolution of around  $\sim 1\text{mm}$  so that the line requirements of  $5\text{mm}$  can realistically be reached.

The fiducial pattern for the pose estimation is chosen to be a *ChArUco* board. It is a combination of a grid of *ArUco* markers and a chessboard pattern, leveraging the speed and reliability of detecting the markers with the high accuracy of detecting chessboard corners. In combination with its robustness to partial views, this pattern

is found to be a good fit for the pose estimation task. The board is glued onto a 0.5mm thin CFRP sheet to provide rigidity and attached to the bottom of the plate.

The choice of image sensor comes down to it having a global shutter to avoid the rolling shutter effect and having a sufficient resolution. The one used is an *OmniVision OV2311* packaged in the *See3CAM 20CUG* camera. As for the lens characteristics, a sufficient depth of field must be reached so that for any position of the plate the fiducial board remains in focus. This is accomplished when the aperture is small and the focal length is short. These characteristics have the welcome side-effect of leading to physically short lenses and a large field of view, which are also required from the lens. The lens with the very smallest aperture and focal length found is chosen, which in this case is the *M12-Lenses PT-01224XFL*. Combined, this image sensor and lens are theoretically able to resolve up to 0.1mm/pixel at the nominal plate distance.

The last component of this assembly is a ring-light placed around the camera to provide even illumination of the fiducial board, which in turn helps with fiducial detection. Since no ring-lights of such a small size could be found, it is made in-house with eight wide-angle white LED's and three stacked diffuser sheets to soften the light.

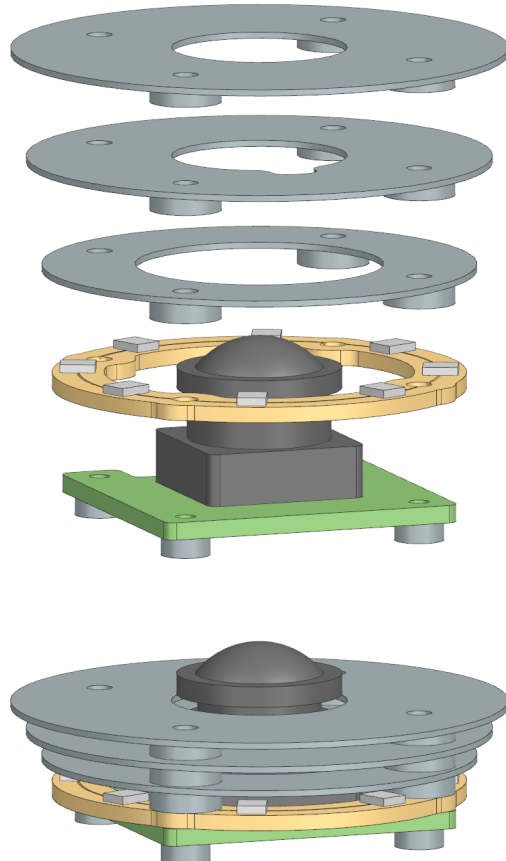


Figure 3.14: Exploded view of the ring-light diffuser

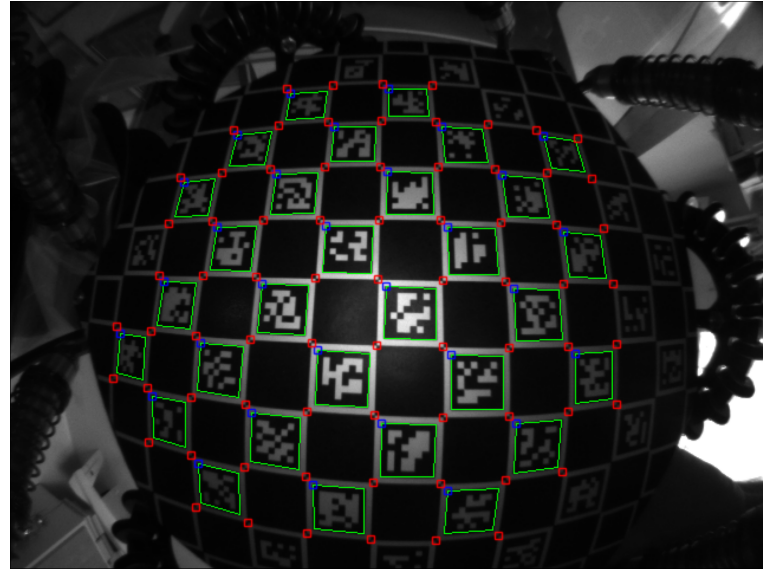


Figure 3.15: Image of camera view with detected *ChArUco* fiducials

For calibration, the camera intrinsics (focal length, distortion, etc.) are determined by recording images of the fiducial board in all its poses and feeding those to the *ChArUco* calibration function. The extrinsics (relative camera position and orientation) are determined by using the *Vicon* motion tracking system to track drone and plate, and picking the extrinsics such that the difference of the two measurements is minimal. The trajectory executed by the plate for this calibration covers its entire movement range in position and in orientation, once slowly and once reasonably fast. Plots of this trajectory can be found at the end of this section.

To judge the performance of the camera tracking the error average (AVG), its variance (VAR) and its 90<sup>th</sup> percentile (P<sub>90%</sub>) are calculated for the position error and the attitude error. Additionally these metrics are calculated for the XY-plane error and yaw error, as these are the measures used for the feedback control.

AVG xyz-error	1.0 mm	AVG xy-error	0.8 mm
STD xyz-error	0.5 mm	STD xy-error	0.5 mm
P <sub>90%</sub> xyz-error	1.7 mm	P <sub>90%</sub> xy-error	1.3 mm
AVG angle-error	0.5 °	AVG yaw-error	0.2 °
STD angle-error	0.4 °	STD yaw-error	0.2 °
P <sub>90%</sub> angle-error	0.9 °	P <sub>90%</sub> yaw-error	0.4 °

Table 3.3: Plate tracking accuracy with camera

It can be noted from the trajectory plots below, that the largest discrepancy between *Vicon* and camera tracking occurs for short durations when the plate moves quickly. This is presumably because the camera tracking is not as fast as the *Vicon* system. Also some error seems to correlate with large deflections, suggesting that the intrinsics calibration could be improved. Nevertheless, these results satisfy the given requirements.

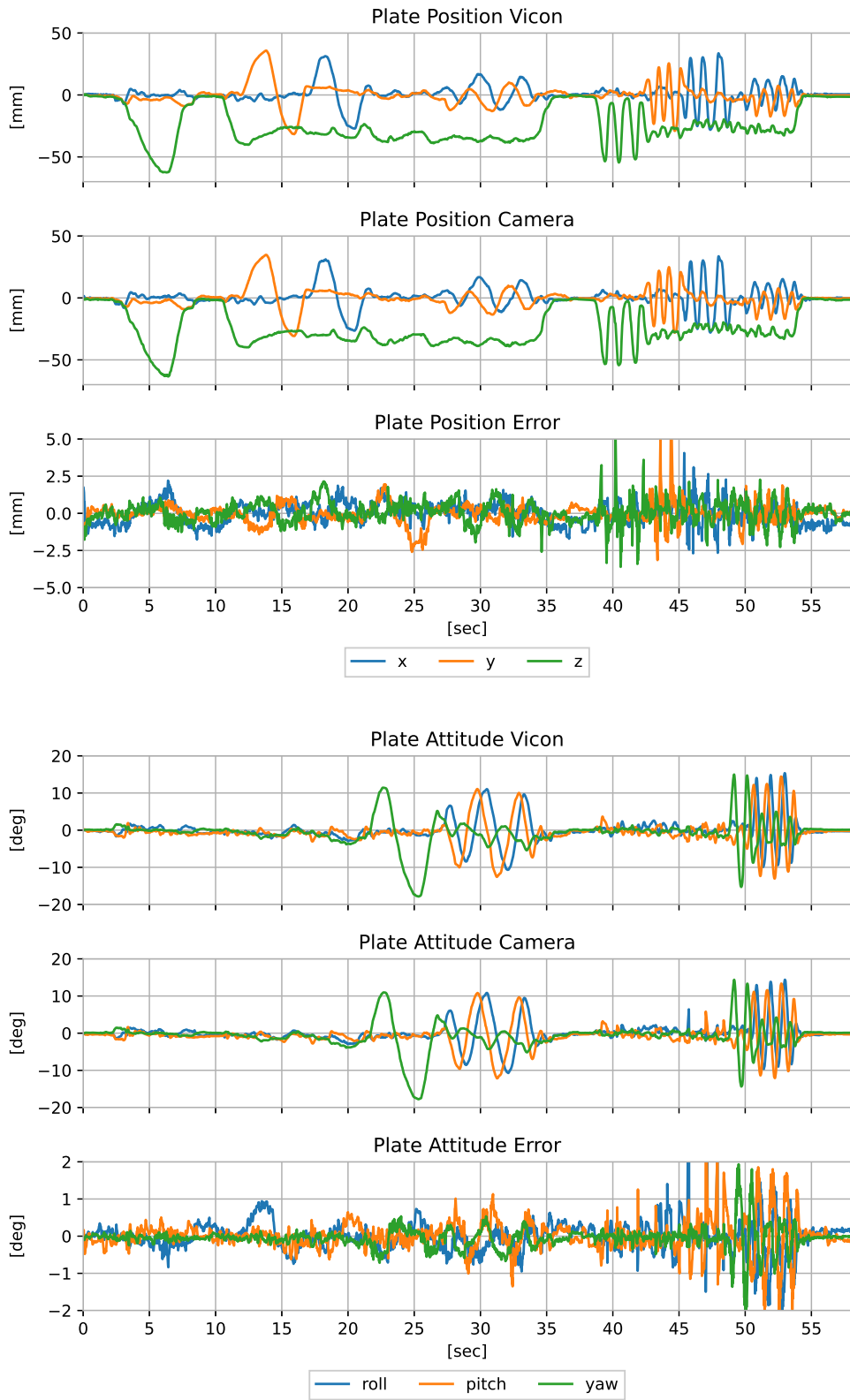


Figure 3.16: Plate trajectory measured with camera compared to *Vicon*

### 3.4 Drawer



Figure 3.17: Image of the finished drawer

The design of the drawer assembly is quite simple and so are its requirements. It has to draw a line of the required width on the ceiling and must be able to start and stop the line at any time without the tool losing ceiling contact.

These requirements are reached by putting a permanent marker in a guiding tube and placing a spring below to push it upwards with  $\sim 0.5\text{N}$ . A small servo motor is attached to the permanent marker through a flexible cable. The cable is flexible so that it becomes taught when the servo retracts, bringing down the permanent marker, but does not interfere with the spring action when the servo is extended.

The permanent marker chosen is an *Edding mini marker 0.5*, producing a 1.2mm line width, used for its short length. While the servo is the ubiquitous *Hitec HS-55*, controlled over USB through an *Adafruit Trinket M0* microcontroller.

Although it is not part of the project requirements, a small endurance test of the permanent marker is performed to determine for how long it can draw when upside down. On paper, with 0.5N force and 20mm/s velocity, the endurance is about 84m before the line quality noticeably degrades.

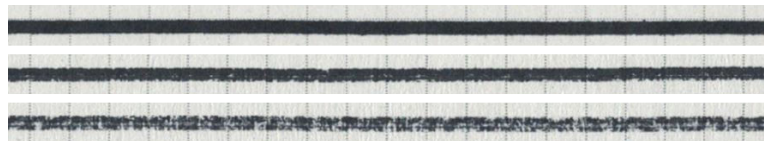


Figure 3.18: Permanent marker line quality after 60m, 84m & 120m

### 3.5 Auxiliary Components

Notable parts of the design that don't belong in any of the above sections are described here. One of them is the cabling. To save weight, all USB cables are collected in a USB-hub on the tool to then connect with a single cable to the drone. In addition every cable is custom made to be as short as possible, including the USB 3.0 cables of the camera and the USB-hub.

A second note regards the two platforms that all components are fixed to. These are 3D printed using carbon fiber reinforced PET-G in a fused deposition printer. Besides being very stiff and lightweight, that material is chosen, because it enables the use of threaded inserts. These allow for easy placement of strong mounting points at any position and angle, and thus let the entire tool easily be disassembled and modified. To further improve weight, while keeping most of the stiffness, only the mounting points and edges of a triangle mesh are printed.

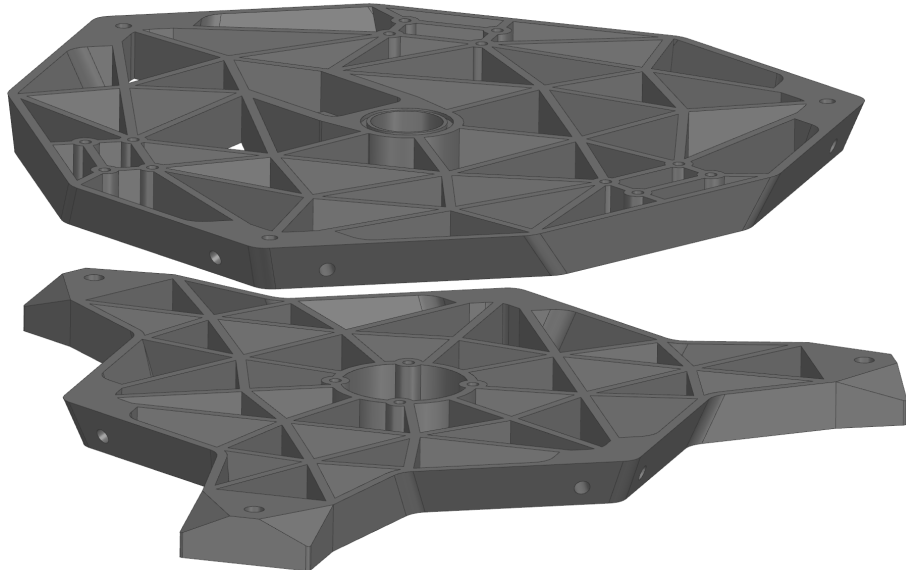


Figure 3.19: Top and bottom platforms of the tool

## 4 Control

The control of the layouting tool is built on top of the Robot Operating System (ROS), as is *Ouzels* flight-controller. This system organizes small programs that perform single tasks in so called nodes (black), which can send messages to each other in so called topics (grey). These nodes are used to interface with the hardware and the user (blue). The graph below shows how the layouting tool controller is organized and connected to the preexisting *Ouzel* controller.

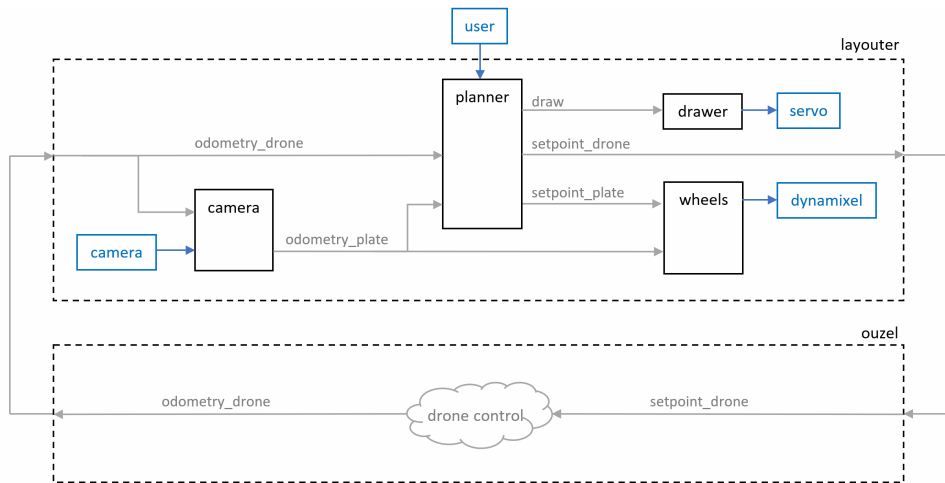


Figure 4.1: Graph of ROS structure

There are two main types of topics being exchanged, the odometry topics holding the current pose of the drone or the plate and the setpoint topics holding the respective desired pose. The "draw" topic simply contains commands to engage and disengage the permanent marker.

For the purpose of this project, *Ouzels* controller is regarded as a black box, since it is not being modified. The nodes relevant for control are the "planner" node, which publishes the setpoints, and the "wheels" node, that uses plate odometry and setpoints to control the wheel actuators. The "camera" and "drawer" nodes won't be discussed further, as their function was already presented in the chapter on design.

## 4.1 Planner Node

The role of the planner node is to, in regular time intervals, calculate where the plate and the drone should be and if a line should be drawn. This trajectory is derived from G-code commands, which are commonly used in computer numerical control (CNC) applications. To keep the node lightweight, a custom interpreter with a reduced instruction set is implemented, that supports the line/arc moves and drawer on/off commands. These commands describe a path in space, but not in time. To handle the timing aspect, an acceleration manager is implemented, that enforces a maximum velocity and acceleration. The manager is able to look ahead on the path and determine when it can accelerate or when it is necessary to start decelerating, so that target velocities can be reached at key locations. Such locations are corners, small radius arcs and drawer on/off locations.

The plots below show the planner output for two trajectories. Each dot represents the XY-coordinate of a published setpoint. Since the setpoints are published in regular intervals, a larger distance between the points implies a greater velocity.

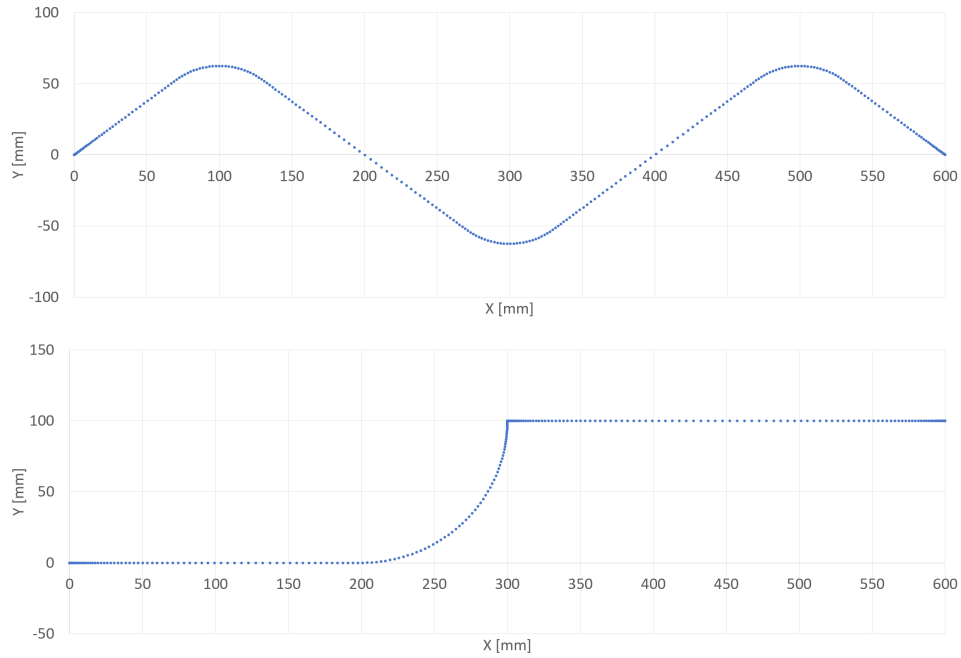


Figure 4.2: Example of two simple plans

The above concerns trajectory planning once in contact with the ceiling. To get into contact in the first place, the planner node features two routines: One to move the drone in free flight to under a starting location and one to drive the drone upwards until the nominal compression of the Stewart platform is reached. At that point the layouting lines can be drawn.

## 4.2 Wheels Node

The wheels node uses the difference between the desired setpoint and the current odometry of the plate to determine how the omni-wheels should move to minimize that difference. A cascaded PID controller is used for this task, due to the simplicity of PID controllers and the improved performance of the cascaded configuration. An outer loop is used to calculate target velocity from position error and an inner loop to calculate target torque from velocity error.

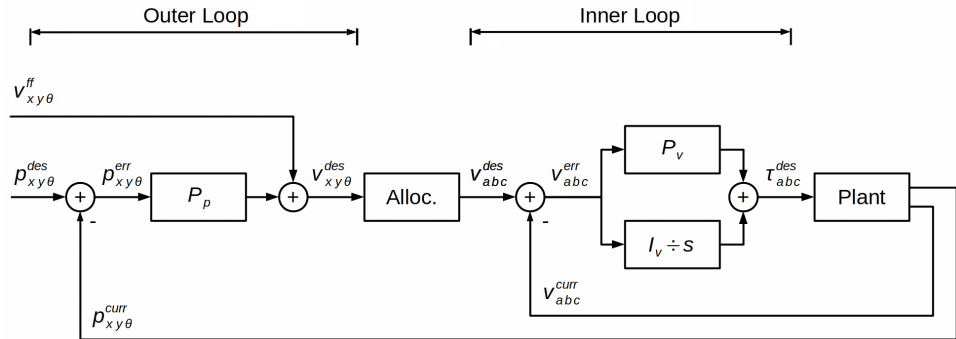


Figure 4.3: Control scheme of the wheel actuators

For the inner loop a proportional-integral PI controller with anti-windup is used that is already built into each *Dynamixel* actuator by default. As such its design is assumed good and only the gains are adjusted. The P & I gains are tuned to be as aggressive as possible without causing instability, as is generally beneficial for cascaded controllers.

The outer loop is designed to be a simple proportional P controller. A differential D term is not needed, as the derivative of position is velocity and that error is already accounted for by the inner loop. An integral I term is deemed unnecessary, as the desired velocity is known and can be passed along as a feed-forward term. Assuming the integrator of the inner loop can avoid static errors in velocity, this means that no major static errors should appear in position either. This controller is tuned after the inner loop controller so that it quickly suppresses position errors without inducing oscillations.

In the implementation, the outer loop uses the linear and angular coordinates  $(x, y, \theta)$  for the plate pose, while the inner loop uses actuator specific coordinates  $(a, b, c)$ . A unique mapping exists between the two thanks to the omni-wheels, that allow for free movement along their main rotation axis, but can enforce movement perpendicular to that direction. The linear coordinates  $x, y$  are allocated to the actuators by projecting them along the enforced travel direction of the matching omni-wheels, while the angular coordinate  $\theta$  is scaled and added to all actuators equally.

## 5 Test-Flights

The test-flights have two main purposes. To determine if the performance requirements can be reached and to validate each of the concept decisions on contact, compliance, actuation and feedback. For this reason tests are flown with the fully assembled layouting tool and with modifications that revert the concept decisions so that their influence can be measured.

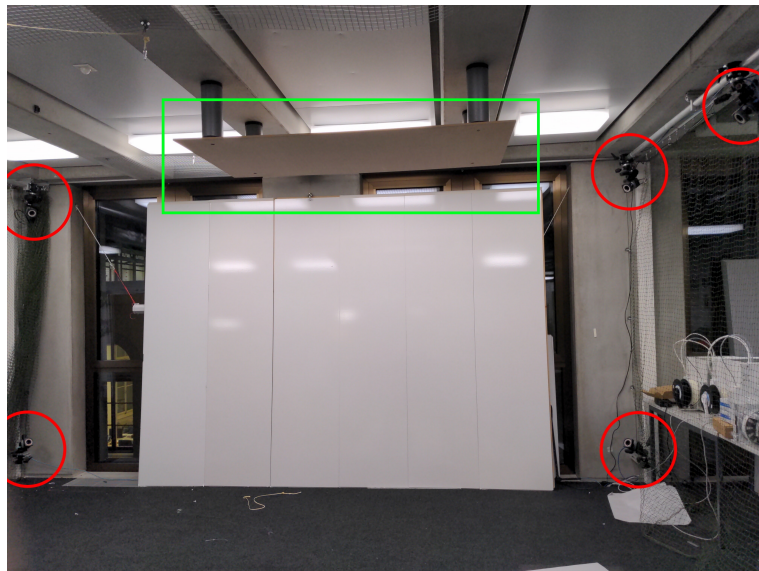


Figure 5.1: Test location with ceiling plate (green) and 5/8 *Vicon* cameras (red)

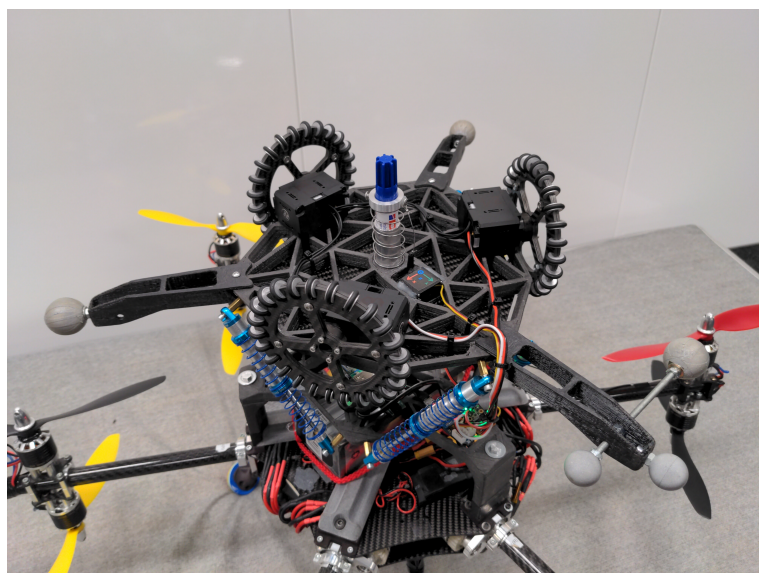


Figure 5.2: Layouting tool with *Vicon* markers fixed to the plate

Common to all test-flights is the trajectory that is drawn. A large circle is used, similar to the one in the Stewart platform dynamics simulation but bigger and traveled much slower to give the best possible results. This shape is chosen for its long length on a small area and its use of all movement directions. The center of the circle is defined as the position where the tool initiates contact with the ceiling, after which it moves to an edge of the circle and starts drawing. The accuracy of the drawn circle is determined by measuring the position of the plate with the *Vicon* tracking system and comparing it with the position setpoints. Three metrics are used to judge performance, the average (AVG) of the error in the XY-plane, its standard deviation (STD) and its 90<sup>th</sup> percentile (P<sub>90%</sub>). The later is deciding on the project success, as the maximum error is most important for the layouting task.

At the end of this chapter some additional raw data of the test-flights is presented. Included is a table showing how the setpoint tracking error of the drone changes in the various tests, a plot showing a top down view of all drawn circles, and the raw flight logs of every test.

Circle diameter	500 mm
Maximum velocity	50 mm/s
Maximum acceleration	25 mm/s <sup>2</sup>

Table 5.1: Test Trajectory Parameters

The various test-flights are performed in an order of increasing complexity. A test in free flight without contact is used as reference for *Ouzels* performance. As a baseline for all following contact tests, the circle is drawn with a marker rigidly fixed to the drone and a single point of contact. Multiple contact points are then introduced by using the omni-wheels without a connected actuator and without the compliance structure. Next, the introduction of the omni-wheel actuators and the Stewart platform compliance are tested separately and then together. The concept decision on feedback is finally tested by comparing performance with a feedforward only omni-wheels controller.

	Drawing on Ceiling	3 Point Contact	Stewart Platform	Omni-Wheel Actuators	Camera Feedback
Free-Flight Test					
Baseline Test	✓				
Contact Test	✓	✓			
Compliance Test	✓	✓	✓		
Actuator Test	✓	✓		✓	(✓)
Feedback Test	✓	✓	✓	✓	
Complete Test	✓	✓	✓	✓	✓

Table 5.2: Test Name vs. Used Components

It can be noticed that not every combination of components is tested. The ones that are skipped are either impossible to test or highly unlikely to work. An obviously impossible test is not having three contact points, but wanting to use the omni-wheel actuators. Also clearly unreasonable are tests where the camera feedback should be used without the omni-wheel actuators and/or without the Stewart platform. A test, whose omission is more more debatable, is to use just 1 contact point together with the Stewart platform. This test is skipped because the Stewart platform adds a lot of freedom of movement to the marker without being particularly strong in stabilizing it, so it's very unlikely that the Stewart platform wouldn't crash into its travel limits.

## 5.1 Free-Flight Test

The free-flight test runs the circle trajectory with the layouting tool mounted, but without any contact with the ceiling. As such it is not drawing anything and can't possibly meet the project requirements. Nevertheless this test gives useful insight when comparing it with the single point of contact of the baseline test. The error of the virtual line, that is traced by projecting the marker position onto the XY plane, is shown in the table below.

AVG xy-error (plate)	22.6 mm
STD xy-error (plate)	13.0 mm
P <sub>90%</sub> xy-error (plate)	43.5 mm

Table 5.3: Free-Flight Test Results (Plate)

In addition to calculating the plate tracking error, this test is also used to validate the presumed drone performance stated in the project framework. For this purpose the position and attitude error of the drone are calculated and listed below. These numbers do match the expectations, but it must again be noted that they do not reflect the peak performance reachable by an OMAV, nor by *Ouzel* specifically. Particularly the angle error is uncharacteristically high for MAVs.

AVG xyz-error (drone)	21.6 mm
STD xyz-error (drone)	9.1 mm
P <sub>90%</sub> xyz-error (drone)	33.8 mm
AVG angle-error (drone)	6.0 °
STD angle-error (drone)	3.0 °
P <sub>90%</sub> angle-error (drone)	11.4 °

Table 5.4: Free-Flight Test Results (Drone)

## 5.2 Baseline Test

The goal of the baseline test is to establish the simplest possible layouting tool design as a comparison point for all modifications that follow. It is a test where the tool has only one contact point to the ceiling, does not have any compliance with respect to the drone and does not have any actuators, nor associated feedback. As such it undoes all concept decisions.

To execute this test a special tool is built out of PET-G with steel rods used as ballast to roughly match the mass and weight distribution of the completed layouting tool. The marker is fixed at the correct height inside a slit tube with a hose clamp. The upward thrust is reduced to 2N for this test, which is approximately the minimum force to maintains ceiling contact. The full 15N that are distributed through the omni-wheels in the other tests are found to be excessive when applied solely through the marker.

AVG xy-error (plate)	40.5 mm
STD xy-error (plate)	27.5 mm
P <sub>90%</sub> xy-error (plate)	87.1 mm

Table 5.5: Baseline Test Results

The line precision in this test is significantly worse than in free-flight. Analysis of the raw odometry data and of video recordings suggests that the cause is the friction at the contact point. This issue exhibits itself in a repeating behaviour, where the marker sticks to the ceiling, the drone pivots around the contact point until the tracking error becomes large enough for the marker to break free and jerk forward a short distance, just to then stick to the ceiling again.



Figure 5.3: Special tool for baseline test

### 5.3 Contact Test

For the contact test the baseline is compared to a configuration with three contact points. To perform this test, the completed layout tool is modified to remove the omni-wheel actuation and the Stewart platform compliance. The actuators are replaced with dummies that don't pose any resistance to turning, while all the spring-dampers are replaced with rigid links matching the nominal length.

The bodies of the dummy actuators are built with a resin 3D printer for increased dimensional accuracy, with threaded inserts matching the mounting points of the real actuator. Deep groove ball bearings are used to enable the shaft to turn freely. For the dummy spring-dampers some aluminium rod is used to connect small ball links that are typically used in model helicopters.

AVG xy-error (plate)	14.5 mm
STD xy-error (plate)	7.9 mm
P <sub>90%</sub> xy-error (plate)	25.0 mm

Table 5.6: Contact Test Results

In this configuration the XY tracking error of the plate is vastly reduced compared to the baseline test. Two mechanisms are thought to be the principal contributors. By using the omni-wheels, much of the friction between ceiling and layout tool is removed, avoiding the issue of the baseline test. Additionally, the three point contact passively stabilizes pitch, roll and z-axis motion. Since it is thought that disturbances in all dimensions are somewhat coupled, stabilizing these should also benefit yaw, x-axis and y-axis precision. The improvement compared to the free-flight test supports this theory.

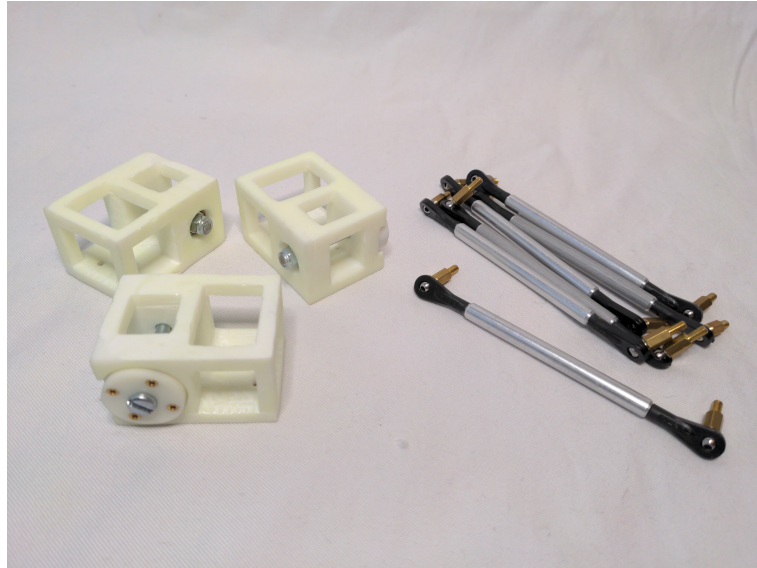


Figure 5.4: Dummy actuators & dummy spring-dampers

## 5.4 Compliance Test

In the compliance test the spring-dampers are introduced. This configuration combines the three contact points with the compliance of the Stewart platform, while leaving the omni-wheels without actuation.

This test is not a fair showcase of the effect of compliance, as the Stewart platform used in this project is designed with actuation in mind. Having no precise plate positioning would require the compliance structure to be designed such that the drone stabilizes the plate instead of the opposite. The XY stiffness would probably also need to be significantly higher. A redesign specifically for this configuration is not performed, because no clear mechanism could be thought of that would predict a tracking error anywhere near the 5mm target.

This test is performed anyways for completeness sake, but the effect of compliance will be judged with the omni-wheel actuators running. The relevant tests are the *actuator test* for actuation without compliance and the *complete test* for actuation with compliance.

AVG xy-error (plate)	33.1 mm
STD xy-error (plate)	15.3 mm
P <sub>90%</sub> xy-error (plate)	54.5 mm

Table 5.7: Compliance Test Results

## 5.5 Actuator Test

For the actuator test the compliance is again removed by installing the rigid dummy spring-dampers. Instead, the real *Dynamixel* actuators are attached to the omni-wheels, enabling the plate to actively drive on the ceiling. In this test the actuators are provided with position feedback, as without compliance the plate pose can be derived from the drone pose, without the need for the camera feedback system.

AVG xy-error (plate)	1.3 mm
STD xy-error (plate)	0.8 mm
P <sub>90%</sub> xy-error (plate)	2.4 mm

Table 5.8: Actuator Test Results

The measured XY plate error demonstrates that this configuration can easily reach the 5mm project goal. Plots of the error show it to be mostly oscillations with a fast frequency of  $\sim 3\text{Hz}$  and no static offset, presumably due to unwanted interaction of the drone and wheels controllers. Since this configuration reaches the goal, it follows that the compliance and associated camera feedback add complexity to the layouting tool that is not necessary. Nevertheless these are still tested to see if they can bring the line precision even lower.

## 5.6 Feedback Test

The feedback test is one step below a complete system test. It includes every element of the concept, except for the camera providing the plate position to the actuators as feedback. As such this test runs the omni-wheel actuators in a feedforward fashion.

AVG xy-error (plate)	33.2 mm
STD xy-error (plate)	25.1 mm
P <sub>90%</sub> xy-error (plate)	69.8 mm

Table 5.9: Feedback Test Results

As could be expected, this configuration performs rather poorly. Two factors are thought to contribute to this result. To turn the wheels in a feedforward manner, the controller uses the omni-wheel diameter to determine the distance traveled, so any error in this diameter will cause increasing drift over distance traveled. The second factor relates to disturbance that can push the plate, and more critically rotate it around its yaw axis. With this control strategy any yaw error rotates the entire trajectory, additionally increasing the setpoint tracking error.

In this test a momentary loss of contact of one omni-wheel is observed due to the very large tracking errors. Following these results, the feedback system is confirmed to be an integral part of the concept when using actuation together with compliance.

## 5.7 Complete Test

For the complete system test the fully assembled layouting tool is used, with all components mounted. This configuration is the most complex one that is tested, but according to the thought process of the concept decisions, also the one that should perform the best. It features the Stewart platform for compliance, the driven omni-wheels for actuation and the camera system to track the position of the plate.

AVG xy-error (plate)	1.0 mm
STD xy-error (plate)	0.5 mm
P <sub>90%</sub> xy-error (plate)	1.7 mm

Table 5.10: Complete Test Results

This configuration manages the lowest line error of all, far below the 5mm target. The error is slightly lower than the actuator test configuration, showing that the Stewart platform does have the intended beneficial effect, even if small. These results also confirm again that the actuated omni-wheels are very effective at improving the drawing precision.

## 5.8 Other Data

In this section a selection of other data is shown, that is not strictly relevant to the project goal. Included is a table showing how the tests influence drone precision, and many raw data plots for the readers to make their own observations.

Test	Plate			Drone					
	xy-error [mm]			xyz-error [mm]			angle-error [deg]		
	AVG	STD	P <sub>90%</sub>	AVG	STD	P <sub>90%</sub>	AVG	STD	P <sub>90%</sub>
Free-Flight	22.6	13.0	43.5	21.6	9.0	33.8	6.0	3.0	11.4
Baseline	40.5	27.5	87.1	21.0	7.7	31.4	13.3	4.3	19.9
Contact	14.5	7.9	25.0	13.2	5.8	20.8	4.0	2.0	7.0
Compliance	33.1	15.3	54.5	15.4	6.2	23.6	6.3	3.9	12.9
Actuator	1.3	0.8	2.4	<b>7.7</b>	<b>1.5</b>	<b>9.8</b>	<b>1.9</b>	<b>0.3</b>	<b>2.4</b>
Feedback	33.2	25.1	69.8	22.4	15.8	44.5	7.1	2.9	11.0
Complete	<b>1.0</b>	<b>0.5</b>	<b>1.7</b>	12.2	3.4	15.6	5.5	1.8	8.5

Table 5.11: Results Table of All Tests

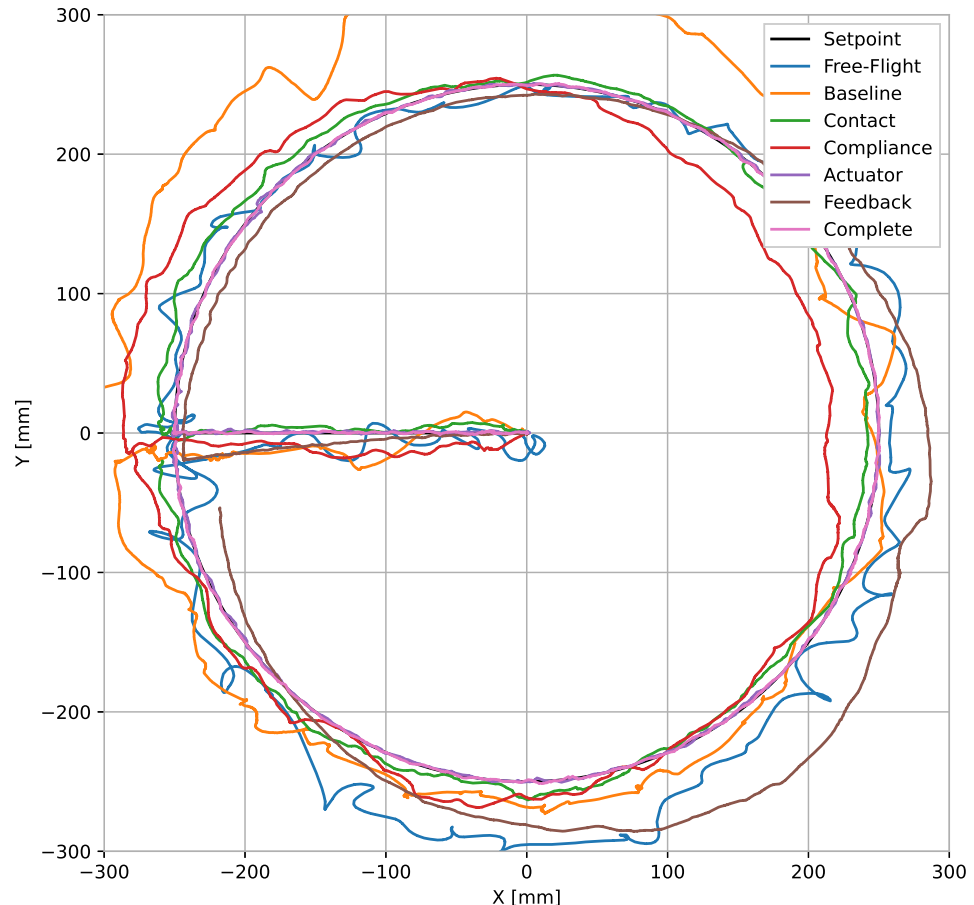


Figure 5.5: Top-Down View of All Tests

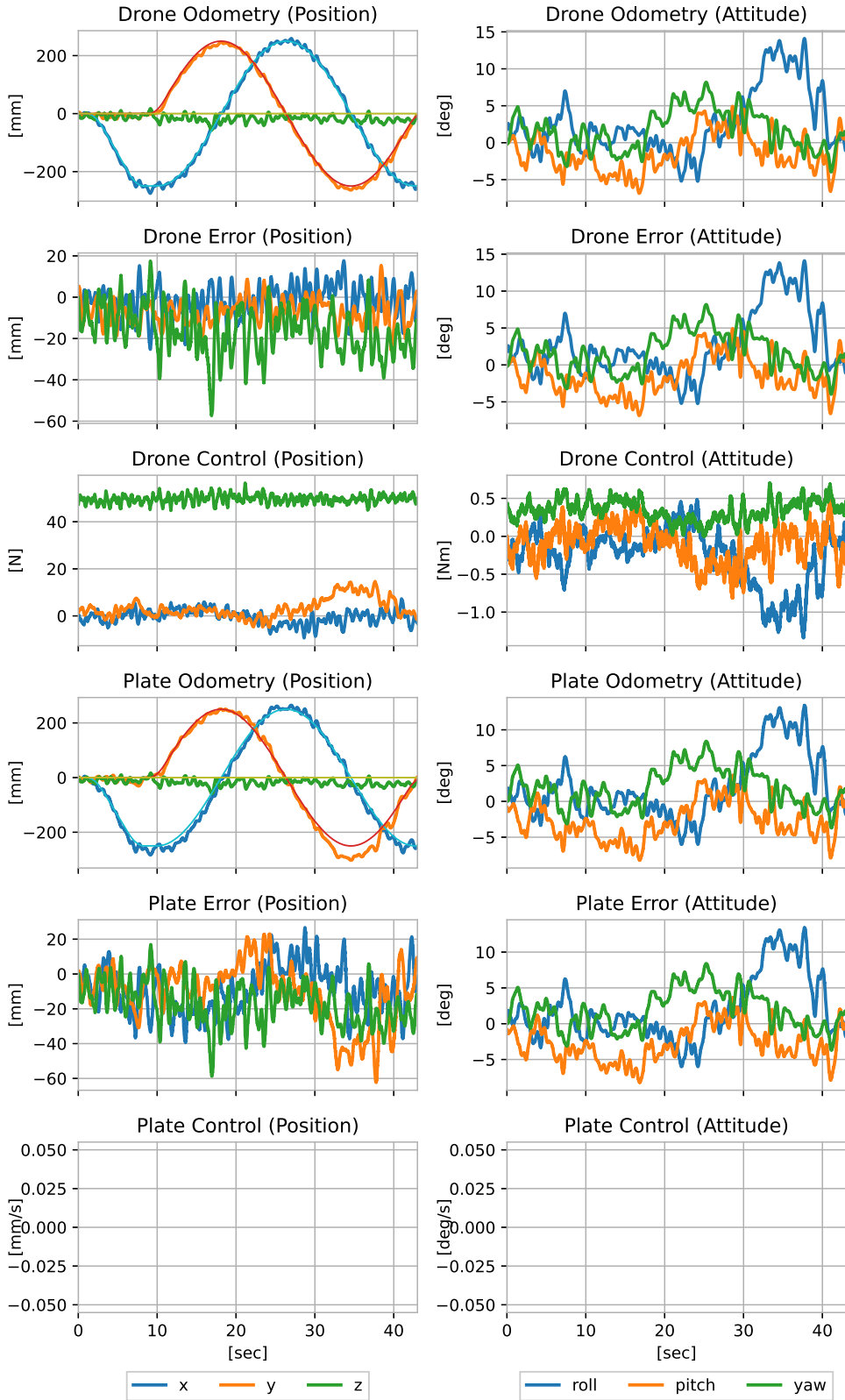


Figure 5.6: Free-Flight Test Data

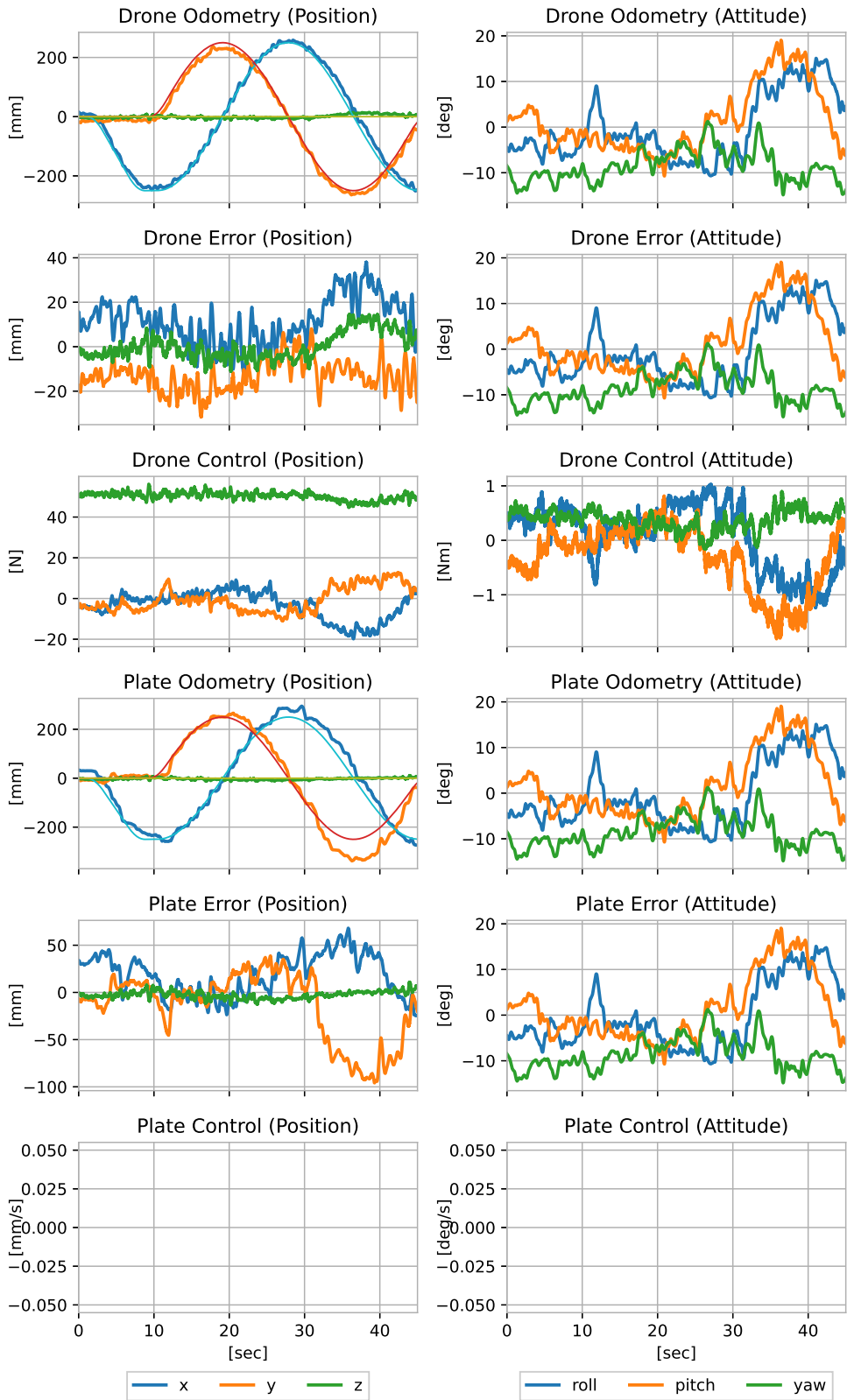


Figure 5.7: Baseline Test Data

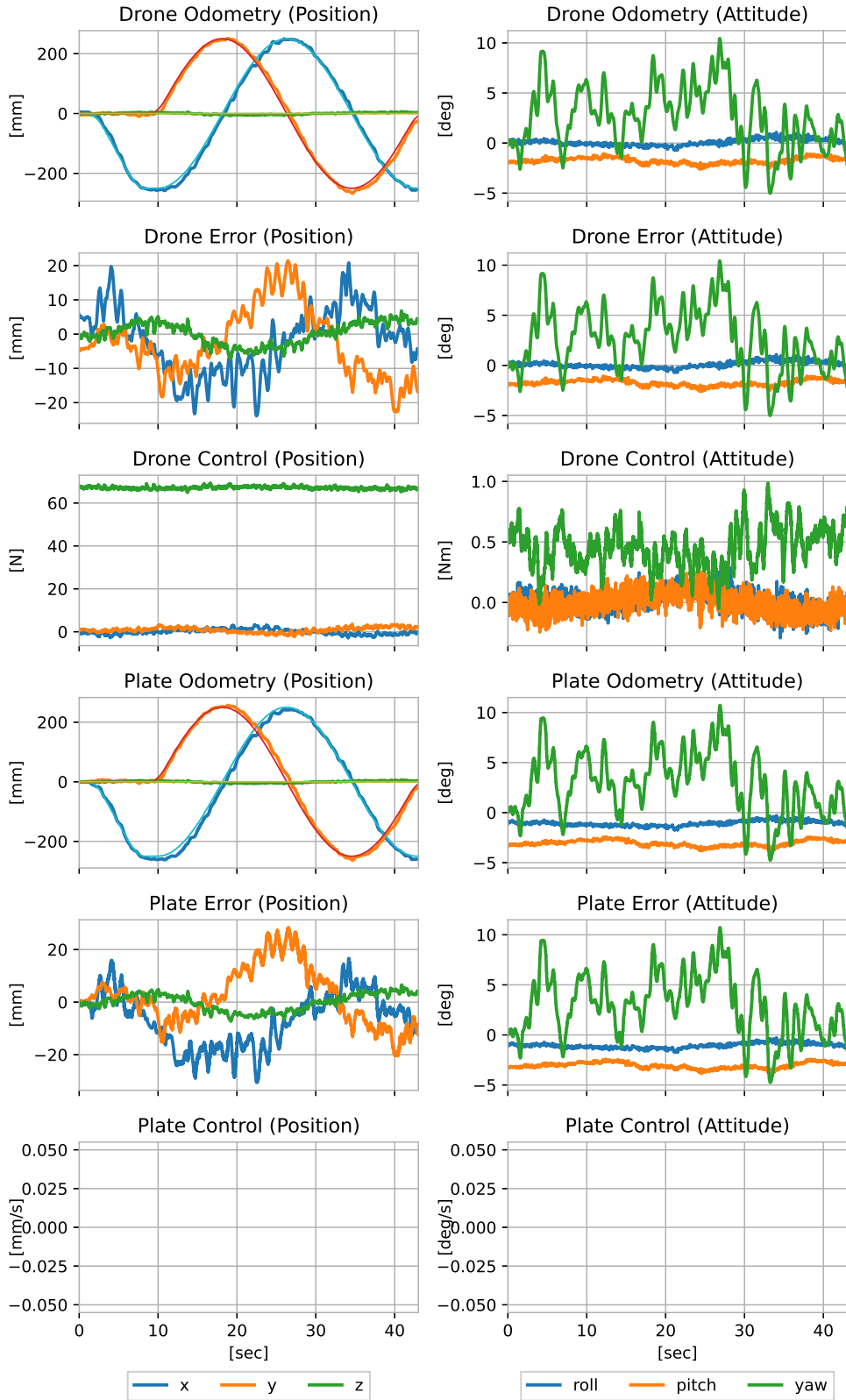


Figure 5.8: Contact Test Data

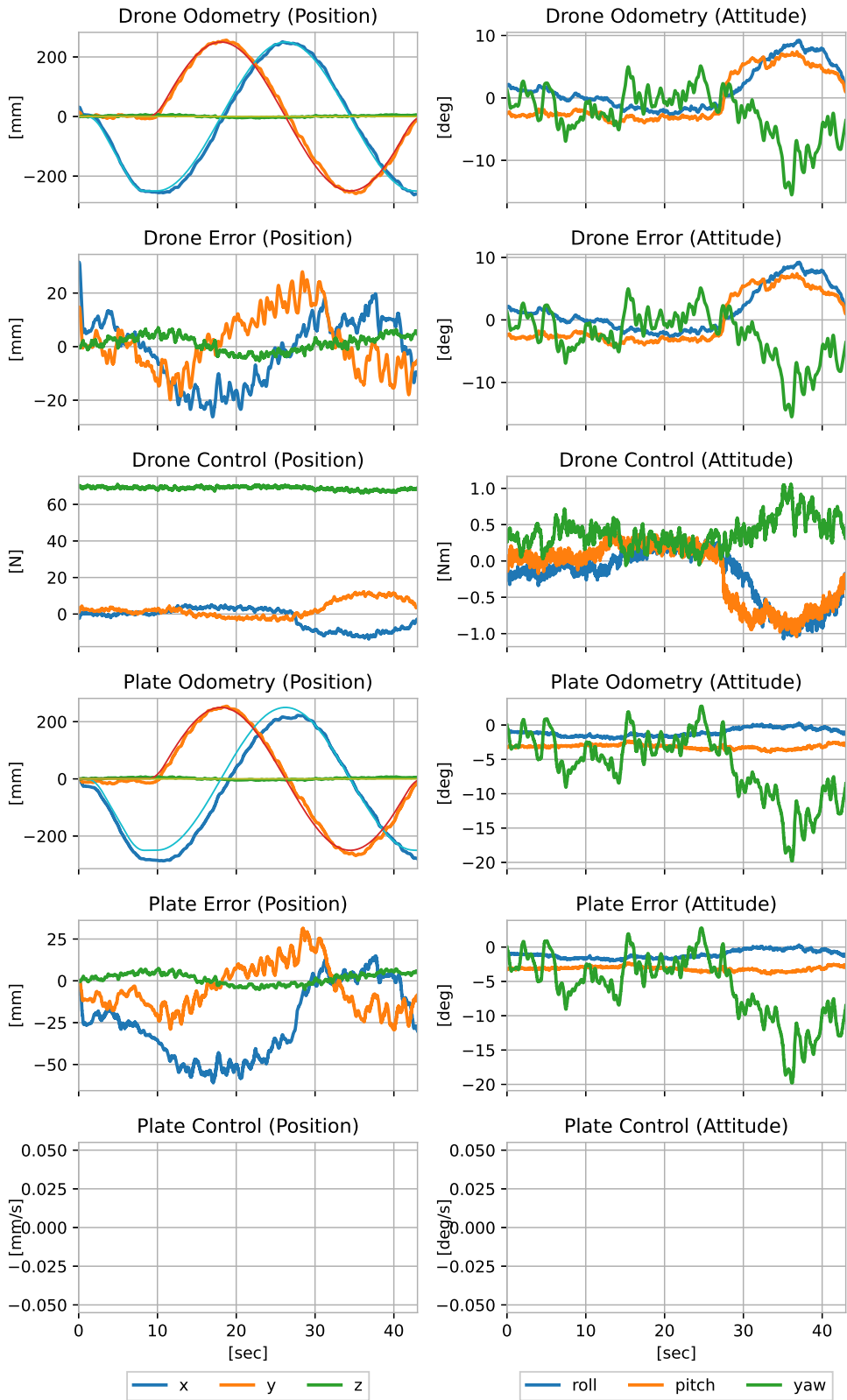


Figure 5.9: Compliance Test Data

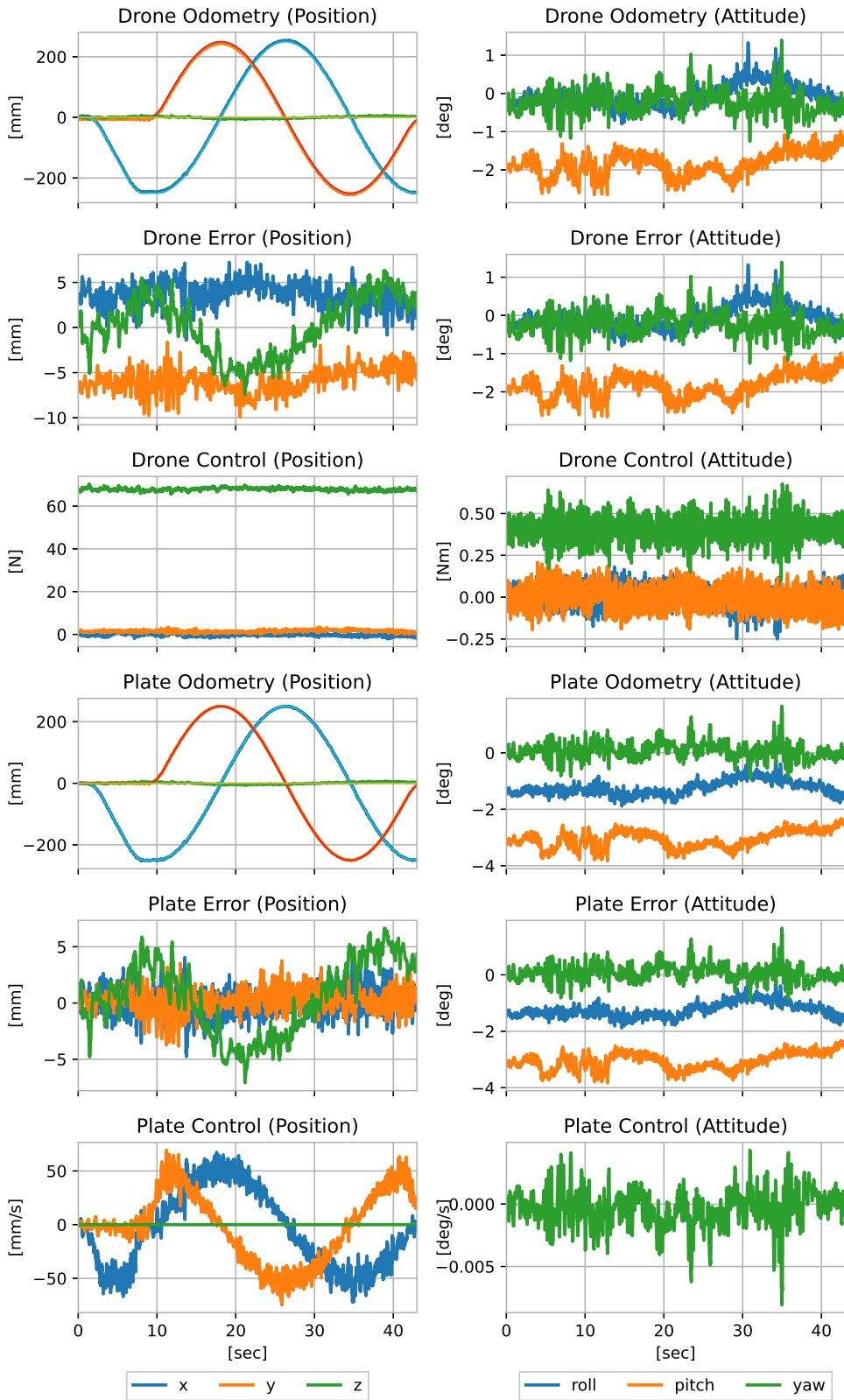


Figure 5.10: Actuator Test Data

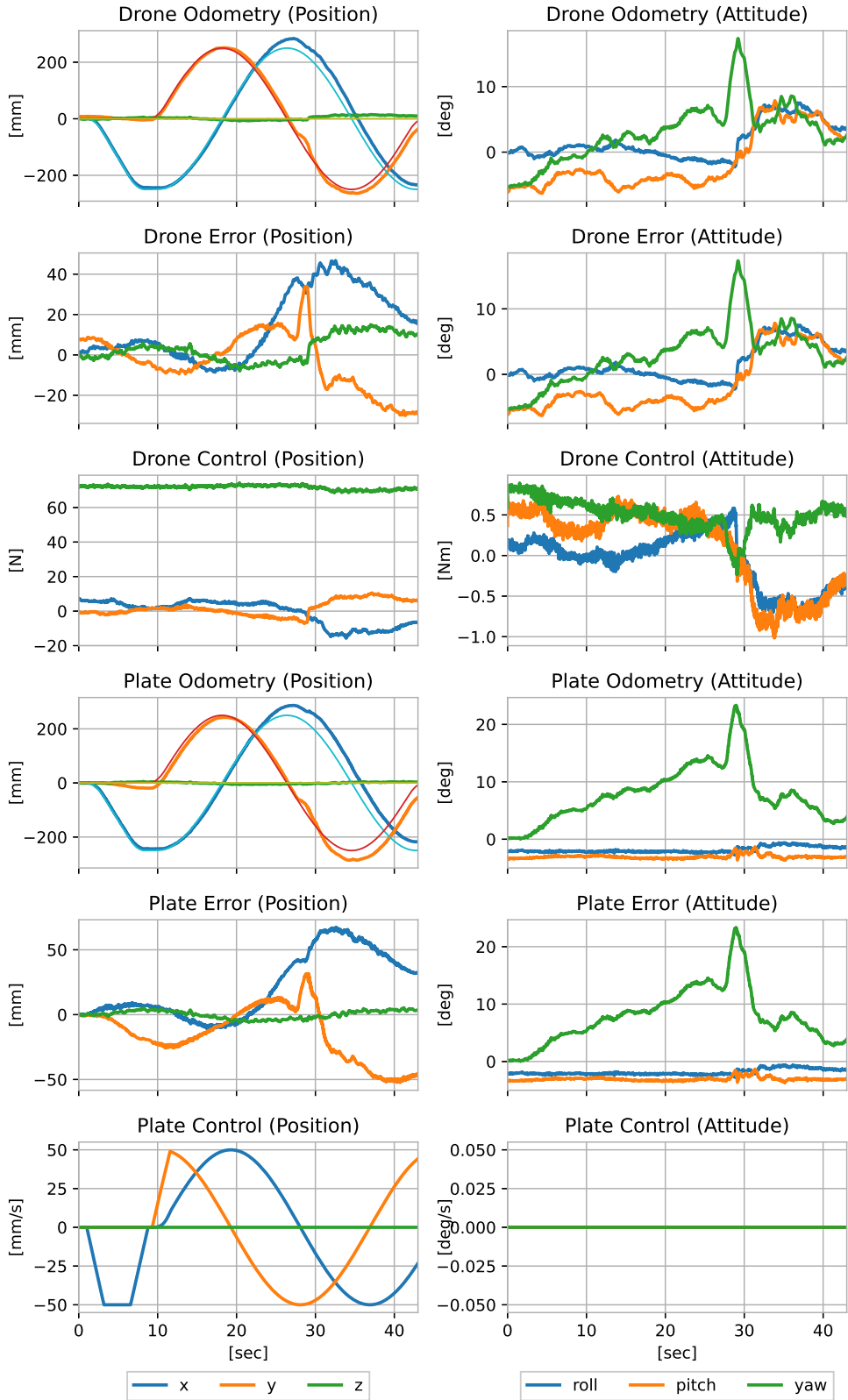


Figure 5.11: Feedback Test Data

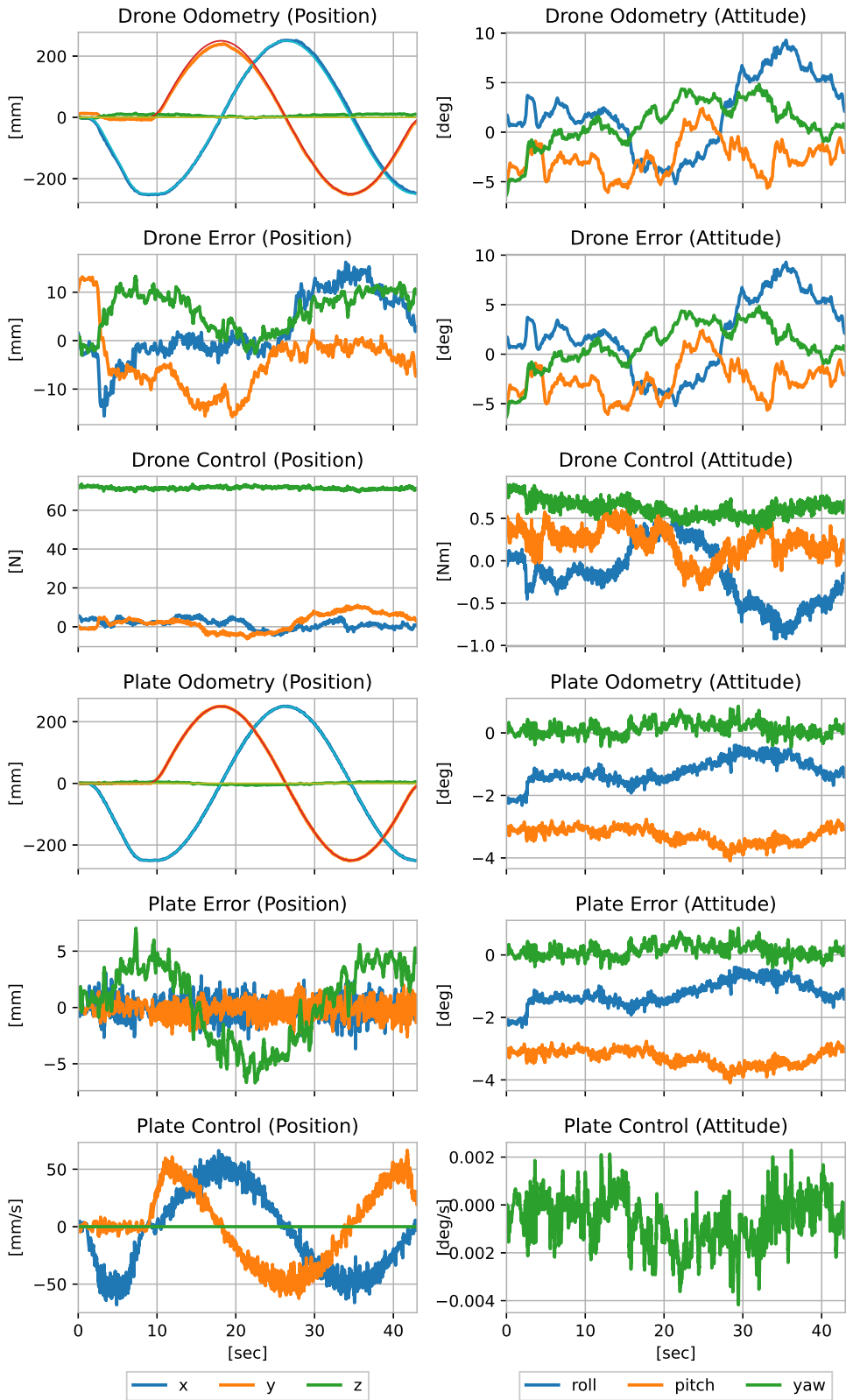


Figure 5.12: Complete Test Data

# 6 Conclusion

This project has found that a layouting tool can be added on top of an OMAV to vastly increase the drawing precision. Despite a setpoint tracking error of the drone in free flight of up to 35mm in position and 10° in attitude, the tool is able to draw lines on a ceiling within no more than 1.7mm error.

The layouting tool manages to do so by providing three points of contact in the form of actuated omni-wheels. These permit the tool to drive on the ceiling, suppressing disturbances and precisely tracking the setpoint. A compliant structure in the form of a Stewart platform with spring-dampers is used between the wheels and the drone. It decouples drone disturbances from the drawing implement. To track the position of the drawer in the challenging environment near the ceiling, a camera pose estimation is used relative to the drone. This position is used as feedback for the omni-wheels.

An alternative design is found that trades in some of the complexity of the tool for a slightly worse drawing accuracy of 2.4mm. This alternative excludes the compliant Stewart platform, also rendering the camera pose estimation unnecessary, and just uses actuated omni-wheels at the ceiling.

To conclude this project the layouting tool is used to draw an actual image on a piece of paper taped to the ceiling. This image is the logo of the Autonomous Systems Lab (ASL), at which this tool was developed.

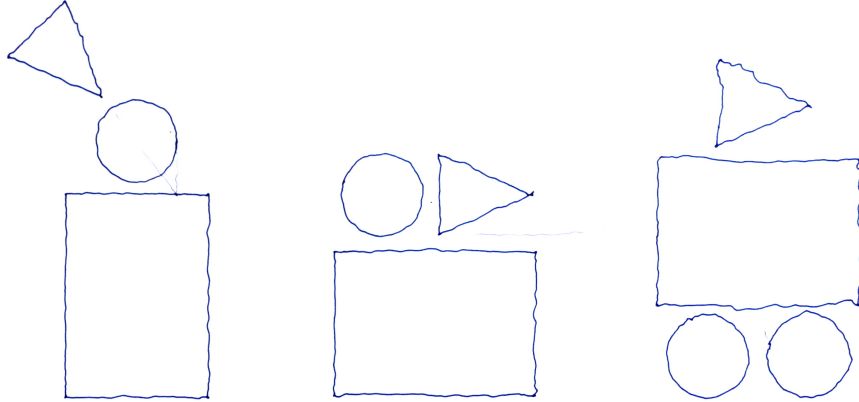


Figure 6.1: ASL logo drawn by the completed layouting tool

The line precision can be seen degrading at the right end, which corresponds to where the drone loses power due to a depleting battery. The drawing is 70cm wide and is performed in 3min 15sec. For the first half of the trajectory a 90th percentile error of 1.5mm is measured by the *Vicon* tracking system at the marker.

## 7 Outlook

While this project was a success in that it reached the goals it set out to, many questions still remain open. One set of these questions regards the design decisions that were not tested for in the test flights. In their defense, the limited amount of man-hours available for this project has restricted the ability to apply a rigorous scientific method to every small decision. Nevertheless the missing tests, that might have improved the performance of the layouting tool, are listed here.

- Test various ceiling forces and damping constants for the Stewart platform
- Test different Stewart platform geometries to validate the simulations
- Test other omni-wheel diameters and different actuators with more torque
- Test the influence saving weight has on the tool

A different kind of interesting questions can be asked if the project framework is loosened slightly to allow for changes to the drone platform *Ouzel*.

- Can *Ouzels* mechanical design be improved to increase drawing precision?
- Can *Ouzels* controller design be improved to increase drawing precision?
- Can *Ouzels* control profit from a force/torque sensor on the layouting tool?
- Can the layouting tool be simplified if *Ouzels* performance is improved?
- Can the layouting tool work on smoothly curved ceilings?
- Can the layouting tool work with a fixed-tilt OMAV or even a traditional multicopter?

Many improvement to the OMAV controller have already been made at the time of writing this report and many more are being worked on in other ASL projects. The mechanical design is also being improved with the upcoming *Quali* OMAV that will replace *Ouzel*. These developments appear to be very promising.

# Bibliography

- [1] K. Bodie, M. Brunner, M. Pantic, S. Walser, P. Pfändler, U. Angst, R. Siegwart, and J. Nieto, “Active interaction force control for contact-based inspection with a fully actuated aerial vehicle,” *IEEE Transactions on Robotics*, vol. 37, no. 3, pp. 709–722, 2021.
- [2] F. Ruggiero, V. Lippiello, and A. Ollero, “Aerial manipulation: A literature review,” *IEEE Robotics and Automation Letters*, vol. 3, no. 3, pp. 1957–1964, 2018.
- [3] D. Xilun, G. Pin, X. Kun, and Y. Yushu, “A review of aerial manipulation of small-scale rotorcraft unmanned robotic systems,” *Chinese Journal of Aeronautics*, vol. 32, no. 1, pp. 200–214, 2019.
- [4] D. Tzoumanikas, F. Graule, Q. Yan, S. Dhruv, M. Popovic, and S. Leutenegger, “Aerial manipulation using hybrid force and position nmpc applied to aerial writing,” *Robotics: Science and Systems XVI*, 07 2020.
- [5] M. Tognon, H. A. T. Chávez, E. Gasparin, Q. Sablé, D. Bicego, A. Mallet, M. Lany, G. Santi, B. Revaz, J. Cortés, and A. Franchi, “A truly-redundant aerial manipulator system with application to push-and-slide inspection in industrial plants,” *IEEE Robotics and Automation Letters*, vol. 4, no. 2, pp. 1846–1851, 2019.
- [6] M. A. Trujillo, J. R. Martínez-de Dios, C. Martín, A. Viguria, and A. Ollero, “Novel aerial manipulator for accurate and robust industrial ndt contact inspection: A new tool for the oil and gas inspection industry,” *Sensors*, vol. 19, no. 6, 2019.

